

RESEARCH ARTICLE

blf and the *drl* cluster synergistically regulate cell fate commitment during zebrafish primitive hematopoiesis

Xue Zhang^{1,*}, Yuxi Yang^{1,*}, Yuxuan Wei¹, Qingshun Zhao¹ and Xin Lou^{2,‡}

ABSTRACT

Hematopoiesis is a highly coordinated process that generates all the body's blood cells, and perturbations in embryonic hematopoiesis may result in illnesses ranging from fetal anemia to various leukemias. Correct establishment of hematopoietic progenitor cell fate is essential for the development of adequate blood cell subpopulations, although regulators of cell fate commitment have not been fully defined. Here, we show that primary erythropoiesis and myelopoiesis in zebrafish embryos are synergistically regulated by *blf* and the *drl* cluster, as simultaneous depletion led to severe erythrocyte aplasia and excessive macrophage formation at the expense of neutrophil development. Integrative analysis of transcriptome- and genome-wide binding data revealed that *blf* and *drl* cluster genes are responsible for constraining the expression of vasculogenesis-promoting genes in the intermediate cell mass and monocytopenia-promoting genes in the rostral blood island. This indicates that *blf* and *drl* cluster genes act as determinants of the fate commitment of erythroid and myeloid progenitor cells. Furthermore, a rescue screen demonstrated that Zfp932 is a potential mammalian functional equivalent to zebrafish *blf* and *drl* cluster genes. Our data provide insight into conserved cell fate commitment mechanisms of primitive hematopoiesis.

KEY WORDS: Hematopoiesis, Zebrafish, Zinc finger protein, *blf*, *drl*

INTRODUCTION

Hematopoiesis in vertebrates, from zebrafish to humans, is an evolutionarily conserved program producing all cellular blood components (Jagannathan-Bogdan and Zon, 2013; Dzierzak and Bigas, 2018; Elsaid et al., 2020). During hematopoiesis, progenitor cells undergo progressive specification and bifurcate into divergent lineages. How blood cell fate divergence is precisely orchestrated has been a topic of much interest because this knowledge is vital to improve our understanding of various blood disorders and to develop new therapeutic strategies.

It is now commonly accepted that hematopoietic cell generation involves bipotent mesodermal precursor cells, the hemangioblasts, which give rise to both hematopoietic and endothelial cells (De Bruijn, 2014). Evidence for the presence of hemangioblasts has been provided by *in vivo* analyses of both mouse and zebrafish embryos (Huber et al., 2004; Vogeli et al., 2006). Transcription

factors, including Tal1, Lmo2, Gata2 and Fli1a, have been suggested to form a recursively wired gene-regulatory circuit to control the emergence of hemogenic endothelium during the early embryonic stages (Pimanda et al., 2007; Lancrin et al., 2009; Carroll and North, 2014; Menegatti et al., 2019). Recent studies have revealed that the initiation of hematopoietic differentiation of hemangioblasts relies on epigenetic regulators, such as Kdm1a (Takeuchi et al., 2015), but it is still largely unknown how presumptive hematopoietic cells shut down endothelial programming to commit to a hematopoietic fate.


In vertebrates, myeloid cells include a diverse repertoire of leukocytes that play essential roles in the immune response, embryogenesis and tissue regeneration (Lavin et al., 2015; Wynn and Vannella, 2016; Watanabe et al., 2019). Based on differences in morphology and biological functions, myeloid cells are classified into two major lineages: granulocytes (neutrophils, basophils and eosinophils), and monocytes/macrophages. In the developing embryo, both lineages are thought to derive from a common myeloid-restricted population termed the neutrophil-macrophage progenitors (NMPs) (Rosenbauer and Tenen, 2007). Recent ontogeny studies have suggested that most tissue-resident macrophages seed the tissues during embryonic development and maintain their pools in the majority of tissues over time (Gomez Perdiguero et al., 2015; Wu and Hirschi, 2020). During zebrafish embryogenesis, myelopoiesis occurs as three distinct waves in a spatially restricted manner. From 12 h post-fertilization (hpf), a population of bipotential myeloid progenitors (marked by *spilb* expression) emerges from the anterior lateral plate mesoderm. Under the control of a highly conserved genetic program, these cells give rise to two major lineages: neutrophils and macrophages (Rosenbauer and Tenen, 2007; Le Guyader et al., 2008; Xu et al., 2012). From around 30 hpf, the intermediate hematopoiesis occurring in the posterior blood island (PBI), produces committed erythromyeloid progenitors (EMPs), which are capable of proliferation and contribute to the erythroid and myeloid lineages (Bertrand et al., 2007; Da'as et al., 2012). Finally, during the definitive wave, hematopoietic stem cells (HSCs) arise from the ventral wall of the aorta then migrate to the caudal hematopoietic tissue where they seed and divide giving rise to all hematopoietic lineages, including myeloid cells (Davidson and Zon, 2004). Previous studies have suggested that granulocyte versus monocyte/macrophage fate determination is primarily governed by the interplay between lineage-specific transcription factors/co-factors and epigenetic modifiers (such as Spi1b, C/EBP α , Irf8, Runx1 and Irf2bp2) and the relative abundances of these determinants at specific developmental stages (Dahl et al., 2003; Li et al., 2011; Jin et al., 2012; Wang et al., 2020). In this way, the molecular mechanisms of NMP cell fate choices are beginning to be understood, although many pieces of this puzzle are still missing.

The zebrafish *bloody fingers* (*blf*) gene encodes a zinc finger family member with multiple sequential C2H2 zinc fingers

¹Medical School, Nanjing University, Nanjing, 210093, China. ²Research Institute of Intelligent Computing, Zhejiang Lab, Hangzhou, 311100, China.

*These authors contributed equally to this work

‡Author for correspondence (xin.lou@zhejianglab.edu.cn)

 Q.Z., 0000-0001-9536-4672; X.L., 0000-0002-6715-0375

Handling Editor: Hanna Mikkola

Received 6 May 2022; Accepted 14 November 2022

spanning almost the entire length of the protein. Although *blf* is specifically expressed in hematopoietic tissues and blood cells (Sumanas et al., 2005), its function in hematopoiesis has not been explored. It has been noticed that *blf* displays sequence homology and an overlapping pattern of expression with *draculin* (*drl*), *draculin-like 1* (*drll.1*), *draculin-like 2* (*drll.2*) and *draculin-like 3* (*drll.3*), four genes clustered consecutively on chromosome 5 with very high sequence homology (Herbomel et al., 1999; Pimpong et al., 2014) (hereafter referred to as the *drl* cluster). Multiple adjacent C2H2 motifs are known to confer DNA-binding activity (Wolfe et al., 2000), suggesting a role for *blf* and *drl* cluster genes as transcriptional modulators. Knockout of *drl* in zebrafish led to a reduction in expression of primitive erythrocyte marker genes (Kobayashi et al., 2020); taking into account the functional redundancy that may exist between *blf* and *drl* paralogs, a more sophisticated strategy is necessary to achieve a comprehensive understanding of the function of this group of genes in hematopoiesis.

In the current study, we provide *in vivo* evidence demonstrating that primary erythropoiesis and myelopoiesis are synergistically regulated by *blf* and *drl* cluster genes. Simultaneous depletion of *blf* and the *drl* cluster led to severe erythrocyte aplasia and excessive macrophage formation at the expense of neutrophil development. Integrative analysis of transcriptome and genome-wide binding data revealed that *blf* and *drl* cluster genes are responsible for constraining the expression of vasculogenesis-promoting genes in the intermediate cell mass and monocytopenia-promoting genes in the rostral blood island. These results indicate that *blf* and the *drl* cluster play important dual roles in cell fate commitment during hematopoiesis: they promote primitive erythropoiesis in hemangioblasts and confer a neutrophil fate on NMPs. Furthermore, we performed a rescue screen and found that Zfp932 is a potential mammalian functional equivalent to zebrafish *blf* and *drl* cluster genes. Our data provide insight into the molecular mechanisms directing primitive erythropoiesis and myelopoiesis.

RESULTS

blf and the *drl* cluster synergistically govern erythropoiesis

In a Tol2 transposon-mediated gene trapping screen to search for regulators of zebrafish embryogenesis (Hou et al., 2017), we identified the RP2-527 line, in which the RFP reporter shows distinct expression patterns in hematopoietic tissues and blood cells (Fig. S1A). 5' RACE was used to identify the gene trapped in the RP2-527 line and sequencing results indicated that the gene-trapping element was integrated within the second intron of the *blf* locus (Fig. S1B). Zebrafish Blf protein contains 15 zinc-finger domains and the insertion resulted in a transcript that encodes a fusion protein containing the first N-terminal 15 amino acids of Blf. Because this fusion protein lacked all zinc-finger domains, the allele that we identified from the RP2-527 line should act as a true null allele. Although previous studies showed that knockdown of *blf* in zebrafish embryos led to defects of morphogenetic movements during neurulation (Sumanas et al., 2005), we did not observe deformity in *blf*^{-/-} embryos or significant effects on overall survival and fecundity of *blf*^{-/-} fish (Fig. S1D). It has been noted that *blf* and *drl* cluster genes may play redundant roles in development because of their high sequence homology and overlapping expression pattern (Sumanas et al., 2005). In order to elucidate the function of this group of genes in development, we used the CRISPR/Cas9 strategy to delete simultaneously four *drl* cluster genes. Multiple sgRNAs targeting 5' and 3' ends of the *drl* cluster were designed (Fig. S2A) and injected into one-cell-stage zebrafish embryos with

Cas9 protein. Among the alleles obtained through this procedure, one bearing a 49,188-bp deletion in the *drl* cluster was chosen to confirm the absence of expression of *drl*, *drll.1*, *drll.2* and *drll.3* (Fig. S2A,B). This allele was assigned as '*drl* 4KO' and used in the subsequent analysis. Embryos from multiple *drl* 4KO heterozygous incrosses were collected and no evident developmental defect was observed in *drl* 4KO homozygous animals (Fig. S2C).

In order to determine whether *blf* and the *drl* cluster synergistically regulate hematopoiesis, *blf*^{-/-}; *drl* 4KO embryos were generated and examined. We first tested whether depletion of *blf* and the *drl* cluster affects primitive erythropoiesis. Whole-mount RNA *in situ* hybridization (WISH) and qPCR revealed that the mature erythrocyte marker *hbae1* was slightly downregulated in *drl* 4KO embryos and almost absent in *blf*^{-/-}; *drl* 4KO samples (Fig. 1A,B). Furthermore, in wild-type, *blf*^{-/-} and *drl* 4KO embryos, hemoglobin-positive cells were found after circulation commenced, but o-dianisidine staining signal was absent in *blf*^{-/-}; *drl* 4KO embryos (Fig. 1A). These results indicated that *blf* and *drl* cluster genes, likely acting in a redundant fashion, regulate primitive erythropoiesis.

Because the expression analysis detected *blf* and *drl* cluster genes in hemogenic endothelial cells (Fig. S1A), we next explored the roles of these genes in definitive erythropoiesis. *In situ* hybridization showed that expression of the HSC marker genes *runx1* and *c-myb* (*myb*) was abolished in *blf*^{-/-}; *drl* 4KO samples but not in *blf*^{-/-} or *drl* 4KO embryos (Fig. 1C). At 7 days post-fertilization (dpf), in contrast to robust o-dianisidine staining of wild-type, *blf*^{-/-} and *drl* 4KO larvae, only sparsely distributed erythrocytes could be observed in *blf*^{-/-}; *drl* 4KO samples (Fig. 1C).

Owing to severe erythrocyte aplasia, *blf*^{-/-}; *drl* 4KO fish exhibited substantial mortality during juvenile stages (Fig. 1D). Approximately 30% *blf*^{-/-}; *drl* 4KO homozygous mutants could be raised to adulthood; we applied microscopic observation and hematological analysis on these animals. The kidneys from *blf*^{-/-}; *drl* 4KO fish were moderately hypoplastic compared with those of controls, and Hematoxylin & Eosin staining revealed that the 'escapers' have an abnormal accumulation of hematopoietic cells between the renal tubules (Fig. S3A,B). This observation was corroborated by differential cell counting, which showed that precursor fractions were markedly increased in *blf*^{-/-}; *drl* 4KO zebrafish compared with controls (Fig. S3C). The peripheral blood from 'escapers' also displayed decreased red blood cell counts, although no appreciable defects of red blood cells were observed (Fig. 1E, Fig. S3D). Taken together, these results indicate that *blf* and *drl* cluster genes are required for normal development of hematopoietic stem cells.

Vertebrate primitive hematopoietic and vascular systems are derived from common precursors, the hemangioblasts (Orkin and Zon, 2008). The expression of *blf* and *drl* cluster genes in the lateral plate mesoderm suggests that the generation of hemangioblasts may be impaired by mutation of these genes. We therefore analyzed expression profiles of three hemangioblast markers, *etsrp*, *lmo2* and *npas4l*, but no differences were observed between wild-type and *blf*^{-/-}; *drl* 4KO embryos (Fig. 2).

It is known that definitive hematopoiesis is associated with arteries (De Bruijn et al., 2002). To establish whether arterial development was affected in *blf*^{-/-}; *drl* 4KO embryos, we determined the expression of arterial marker genes and examined vascular development with alkaline phosphatase staining and the *Tg(kdrl:EGFP)*^{s843} line. No obvious difference in these assays was observed between *blf*^{-/-}; *drl* 4KO and control embryos

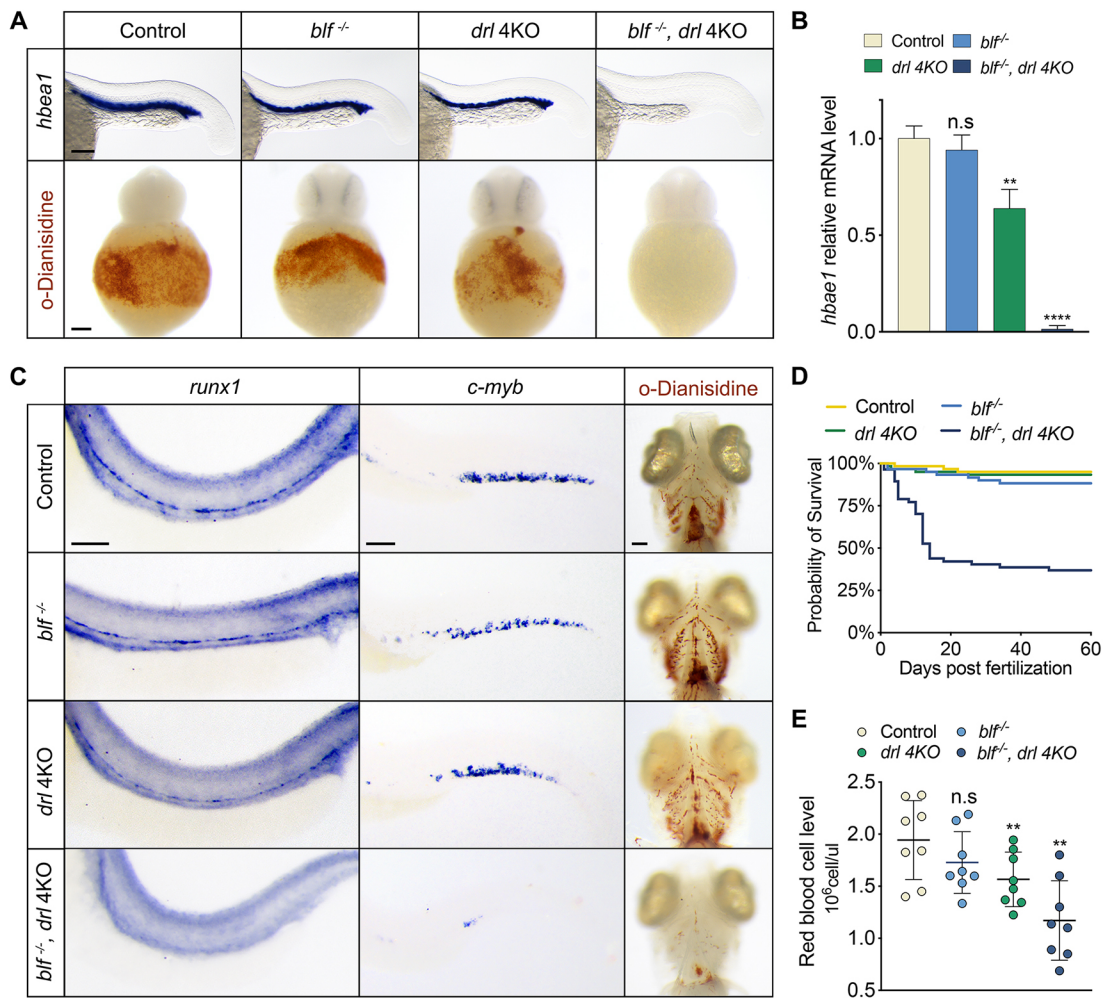


Fig. 1. Simultaneous depletion of *blf* and the *drl* cluster leads to severe erythrocyte aplasia. (A) Top: RNA *in situ* hybridization of *hbae1* expression in primitive erythrocytes of 23 hpf embryos. Bottom: Whole-mount o-dianisidine staining of 36 hpf embryos. (B) Relative expression levels of *hbae1* in 23 hpf embryos. Data are mean±s.e.m. (C) Left: RNA *in situ* hybridization of *runx1* expression in the dorsal aorta of 36 hpf embryos. Middle: RNA *in situ* hybridization of *c-myb* expression in the caudal hematopoietic tissue of 3 dpf embryos. Right: Whole-mount o-dianisidine staining of 7 dpf embryos; ventral views. (D) Representative Kaplan–Meier plot for wild-type, *blf*^{-/-}, *drl* 4KO and *blf*^{-/-}; *drl* 4KO fish from one of three independent experiments. Eighty animals of each genotype were followed. (E) Red blood cell levels in peripheral blood from adult fish; data are mean±s.e.m. Circles represent individual samples. In B and E, n.s., not significant, ***P*<0.01, *****P*<0.0001. Scale bars: 100 μm.

(Fig. S4). This result implies that the *blf* and *drl* cluster genes are dispensable for hemangioblast formation and vasculature development.

In zebrafish, primitive erythropoiesis takes place in the intermediate cell mass region and a sophisticated network of transcription factors and epigenetic regulators has been described as regulating this process (Wells and Steiner, 2022). To assess the state of the hematopoietic transcription network in *blf*^{-/-}; *drl* 4KO embryos, the expression of *gata1*, *trim33* and *tall1* was analyzed and demonstrated to be greatly reduced (Fig. 3A). By utilizing RFP expression from the *blf* gene-trapping allele as lineage tracer, we examined erythroid progenitors in live embryos. Confocal microscopy images showed that primitive erythroid progenitors displayed a uniformly round shape in control embryos. Conversely, erythroid progenitors in *blf*^{-/-}; *drl* 4KO embryos exhibited irregular shape and size, and RFP-positive puncta could be observed in these cells (Fig. 3B,C). These observations prompted us to examine the viability of erythroid progenitors in *blf*^{-/-}; *drl* 4KO embryos. TUNEL staining revealed that differentiating erythroid cells in both the intermediate cell mass and the erythro-myeloid progenitor

population undergo enhanced programmed cell death in *blf*^{-/-}; *drl* 4KO embryos (Fig. 3D,E). All of these results indicate that *blf* and *drl* cluster genes are essential for the differentiation and survival of primitive erythrocytes.

***blf* and *drl* cluster genes regulate neutrophil versus macrophage fate choice during primitive myelopoiesis**

Gene expression analysis showed that both *blf* and *drl* cluster genes were present in myelopoietic tissues, including the rostral blood island (Fig. S1A; Pimpong et al., 2014); this prompted us to study the role of these genes in myelopoiesis. We first assessed early myeloid cell specification using WISH and qPCR for *spi1b*. At the 10-somite stage (14 hpf), there was no notable difference in the expression of *spi1b* in *blf*^{-/-}; *drl* 4KO or *blf*^{-/-}; *drl* 4KO mutants compared with the wild type (Fig. S5A). To assess the effect of loss of *blf* and *drl* cluster genes on primitive granulopoiesis and monopoiesis, we performed WISH for myeloid marker genes. The data showed that in *blf*^{-/-}; *drl* 4KO mutants the number of differentiating neutrophils (marked by *mpx* and *lyz* expression) was greatly decreased, whereas the number of macrophages

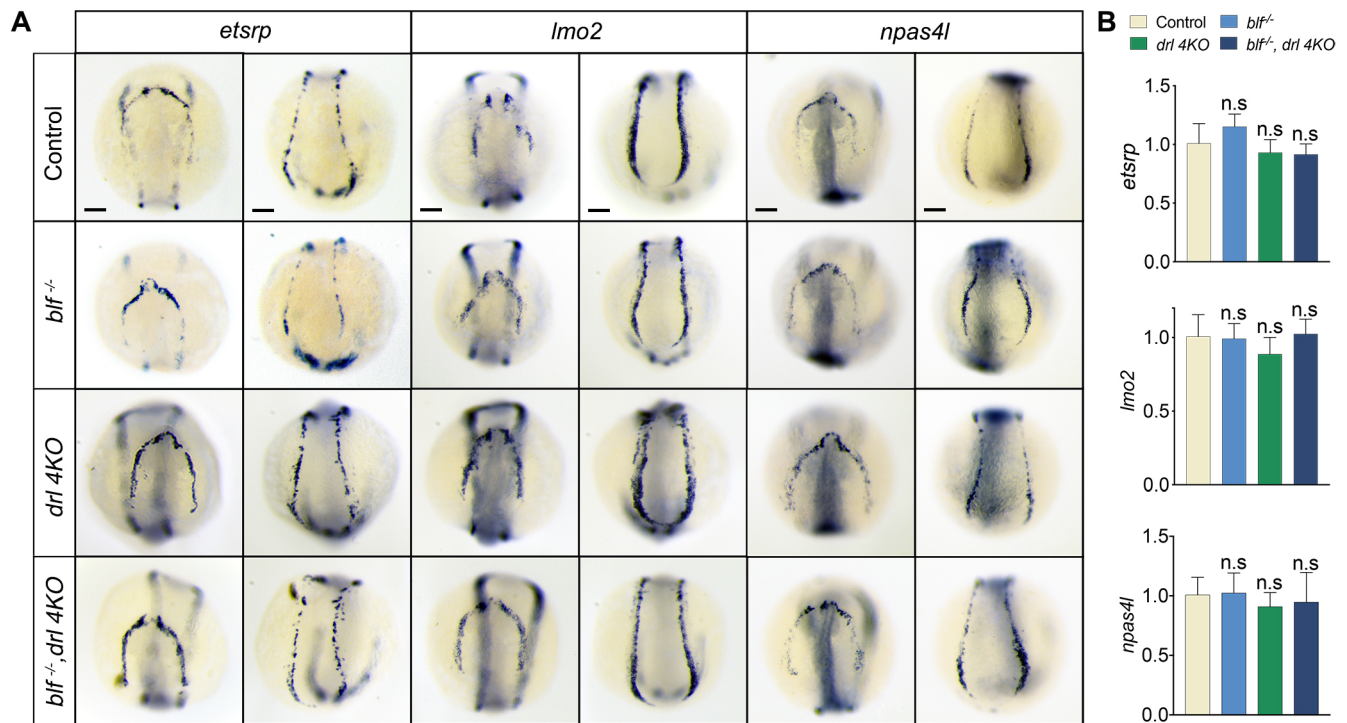


Fig. 2. *blf* and *drl* cluster genes are dispensable for hemangioblast formation. (A) RNA *in situ* hybridization of *etsrp*, *lmo2* and *npas4l* expression in 8-somite embryos. For *etsrp* WISH, $n=28, 33, 36$ or 32 . For *lmo2* WISH, $n=37, 25, 32$ or 29 . For *npas4l* WISH, $n=32, 29, 27$ or 25 . Listed sample sizes relate to each group shown from top to bottom. (B) qPCR results for expression of *etsrp*, *lmo2* and *npas4l* in 8-somite embryos. Data are means \pm s.e.m. of at least three replicates. n.s., not significant. Scale bars: 100 μ m.

(distinguished by *mpeg1* and *mfap4.1* expression) was mildly increased (Fig. 4A). To investigate the possible mechanism, we examined cell numbers of the entire myeloid population. The overall number of cells positive for *coro1a*, a pan-myeloid marker identifying all myeloid subsets (Li et al., 2012), was comparable between *blf*^{-/-}; *drl* 4KO mutants and control embryos (Fig. 4A). To investigate further the role of *blf* and *drl* cluster genes in the fate decision of primitive myeloid progenitors, we examined the proportion of progenitors taking the path of granulopoiesis or monocytopenesis. To do this, hematopoietic cells in the rostral blood island were labeled with uncaging photoactivatable fluorescein (Flu) at 20 hpf (Fig. S6), and the contribution to neutrophils or macrophages was determined by double staining against Flu and mRNA of marker genes at 72 hpf. The data showed that in control embryos the myeloid progenitors from the rostral blood island have a similar probability to differentiate into neutrophils or macrophages. By contrast, in *blf*^{-/-}; *drl* 4KO embryos the vast majority of myeloid progenitors give rise to macrophages and only very small fraction of them adopt the neutrophil fate (Fig. 4B). This supports the notion that imbalanced myeloid lineage development could be caused by expansion of the macrophage population at the expense of neutrophil development.

To evaluate the roles of *blf* and *drl* cluster genes in intermediate myelopoiesis, we examined the expression of *gata1* and *lmo2* at 30 hpf. Loss of *blf* and *drl* cluster genes abolished the expression of these two genes in the PBI, indicating that the formation of EMPs was severely defective (Fig. S5B). In agreement with this result, in the PBI of *blf*^{-/-}; *drl* 4KO mutants the number of cells positive for *mpx* or *mpeg1* expression was also profoundly lower and the decreased neutrophil population was further confirmed by Sudan Black staining (Fig. S7). In further analysis of the definitive wave of myelopoiesis, WISH results showed that at 96 hpf the number of

both *mpx*-positive neutrophils and *mpeg1*-positive macrophages in *blf*^{-/-}; *drl* 4KO mutants was lower than that in controls (Fig. S8).

Collectively, these data showed that the loss of *blf* and *drl* cluster genes leads to aberrant neutrophil versus macrophage fate decision during primitive hematopoiesis and drastic defects in intermediate and definitive myelopoiesis.

***blf* and *drl* cluster genes redundantly regulate zebrafish hematopoiesis**

To confirm that the *blf* and *drl* cluster genes act in a redundant fashion, we tested the efficacy of *blf* and four *drl* cluster genes in rescuing defective hematopoiesis in *blf*^{-/-}; *drl* 4KO embryos. By microinjection, mRNA of individual genes was introduced back into *blf*^{-/-}; *drl* 4KO embryos and primary erythropoiesis and myelopoiesis were analyzed with qPCR, WISH and o-dianisidine staining. The results showed that all five genes could partially restore both erythropoiesis and granulopoiesis in *blf*^{-/-}; *drl* 4KO embryos, with *drl* displaying the highest potency (Fig. S9).

***blf* and *drl* cluster genes govern cell fate commitment during primitive erythropoiesis and myelopoiesis**

blf and *drl* cluster genes encode transcription factors with multiple sequential C2H2 zinc fingers, and we performed integrative analysis on their transcriptome and genome-wide binding profile to investigate how these proteins modulate the transcriptional program in hematopoietic progenitors. In order to determine how loss of *blf* and *drl* cluster genes changes the transcriptome landscape, hematopoietic progenitors were collected by fluorescence-activated cell sorting (FACS) by utilizing RFP expression from the *blf* gene-trapping allele as lineage tracer, and low input RNA sequencing (RNA-seq) was carried out (Fig. S10). In hematopoietic progenitors from *blf*^{-/-}; *drl* 4KO embryos, a total

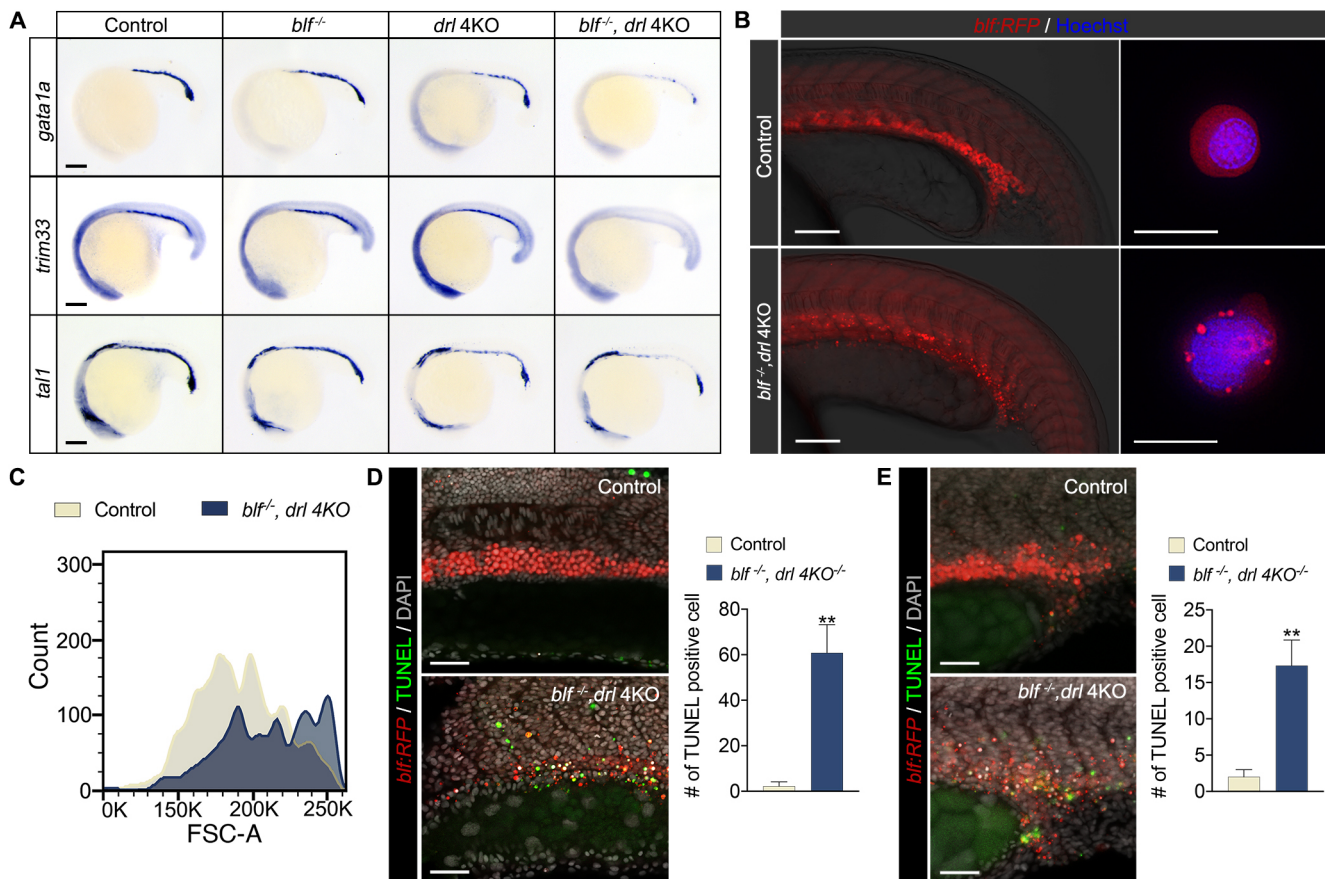


Fig. 3. *blf* and *drl* cluster genes are essential for establishing the erythroid cell differentiation program. (A) RNA *in situ* hybridization of *gata1a*, *trim33* and *tal1* expression in 18-somite embryos. Lateral view with head to left. For *gata1a* WISH, $n=37, 35, 33$ or 36 . For *trim33* WISH, $n=40, 38, 37$ or 32 . For *tal1* WISH, $n=31, 25, 40$ or 37 . Listed sample sizes relate to each group shown from top to bottom. Scale bars: $100\ \mu\text{m}$. (B) Fluorescence micrographs of control (*blf*^{-/-}) and *blf*^{-/-}; *drl* 4KO embryos and sorted RFP⁺ cells at 22 hpf. Scale bars: $200\ \mu\text{m}$ (left); $10\ \mu\text{m}$ (right). (C) Histograms of forward scatter showing approximate cell size distributions of the sorted RFP⁺ cells. (D, E) Left: Cell death in the intermediate cell mass (D) and in EMPs (E) assessed with TUNEL staining at 22 hpf. Scale bars: $100\ \mu\text{m}$. Right: Quantification of TUNEL-positive cells counted on a $100\ \mu\text{m}\times 250\ \mu\text{m}$ field for inner cell mass and $125\ \mu\text{m}\times 125\ \mu\text{m}$ field for EMPs. Data are mean \pm s.e.m. ** $P<0.01$. Data were collected for 8-12 samples per experiment group.

of 1516 genes, consisting of 375 with decreased and 1141 with increased expression, were significantly altered [\log_2 (fold change) >2 , false discovery rate (FDR) <0.001] (Table S1). The majority of the aberrantly expressed genes were upregulated rather than downregulated in the *blf*^{-/-}; *drl* 4KO samples, suggesting that *blf* and *drl* cluster genes may primarily act as transcription repressors (Fig. 5A). Gene ontology (GO) enrichment analysis revealed that genes deregulated in *blf*^{-/-}; *drl* 4KO samples were involved in erythrocyte and myeloid cell differentiation, vasculature development, Notch signaling, cell migration and metabolism of extracellular matrix (Fig. 5B). These findings were further confirmed by gene set enrichment analysis (GSEA), an independent, unbiased approach analyzing enrichment of functional groups, and a similar set of pathways was detected (Fig. 5C, Fig. S11). Moreover, qPCR of representative genes from enriched gene sets was applied to support the reliability of the expression data obtained by low-input RNA-seq (Fig. 5D).

To investigate the *blf* and *drl* cluster regulatory network and associated mechanisms of action, we used cleavage under targets and tagmentation (CUT&Tag) technology to determine their genome-wide occupancy in hematopoietic progenitors. To recapitulate the physiological binding profile, mRNA coding Blf-3xFLAG or Drl-3xFLAG was injected into *blf*^{-/-}; *drl* 4KO embryos and hematopoietic progenitors were purified using RFP as a lineage

tracer at 20 hpf. To reduce the number of embryos required, we used the CUT&Tag procedure, which has proven highly efficient for globally identifying binding sites in low-input samples (Kaya-Okur et al., 2020; Li et al., 2021). Following next-generation sequencing, analysis of the CUT&Tag data resulted in the identification of 10,267 and 6394 high-confidence binding sites for Blf and Drl, respectively (Table S2), which provided an estimate of the number of genomic positions occupied by Blf or Drl in hematopoietic progenitors at this stage of development. The peaks were enriched in gene promoter regions (demarcated here as $\pm 3\ \text{kb}$ from the TSS; Fig. 6A,B), but a significant portion of Blf and Drl binding sites also localized to distal intergenic regions, suggesting that they direct transcription regulation at both promoters and enhancers (Fig. 6B). There was extensive overlap (63.9%) between Blf and Drl chromatin occupancy, as well as substantial overlap (65.7%) between their associated genes (Fig. 6C), indicating that they are involved in an interwoven regulatory network. DNA-binding motifs for other hematopoietic transcription regulators, including CEBP, GATA factors and KLF factors, were enriched on the overlap peaks (Fig. S12), implying cooperation between Blf/Drl genes and these hematopoietic factors. To determine enriched DNA motifs at Drl occupancy sites, *de novo* motif analysis was performed with the HOMER tool and a set of potential Drl binding motifs was identified (Fig. 6D). To identify the direct targets and mode of

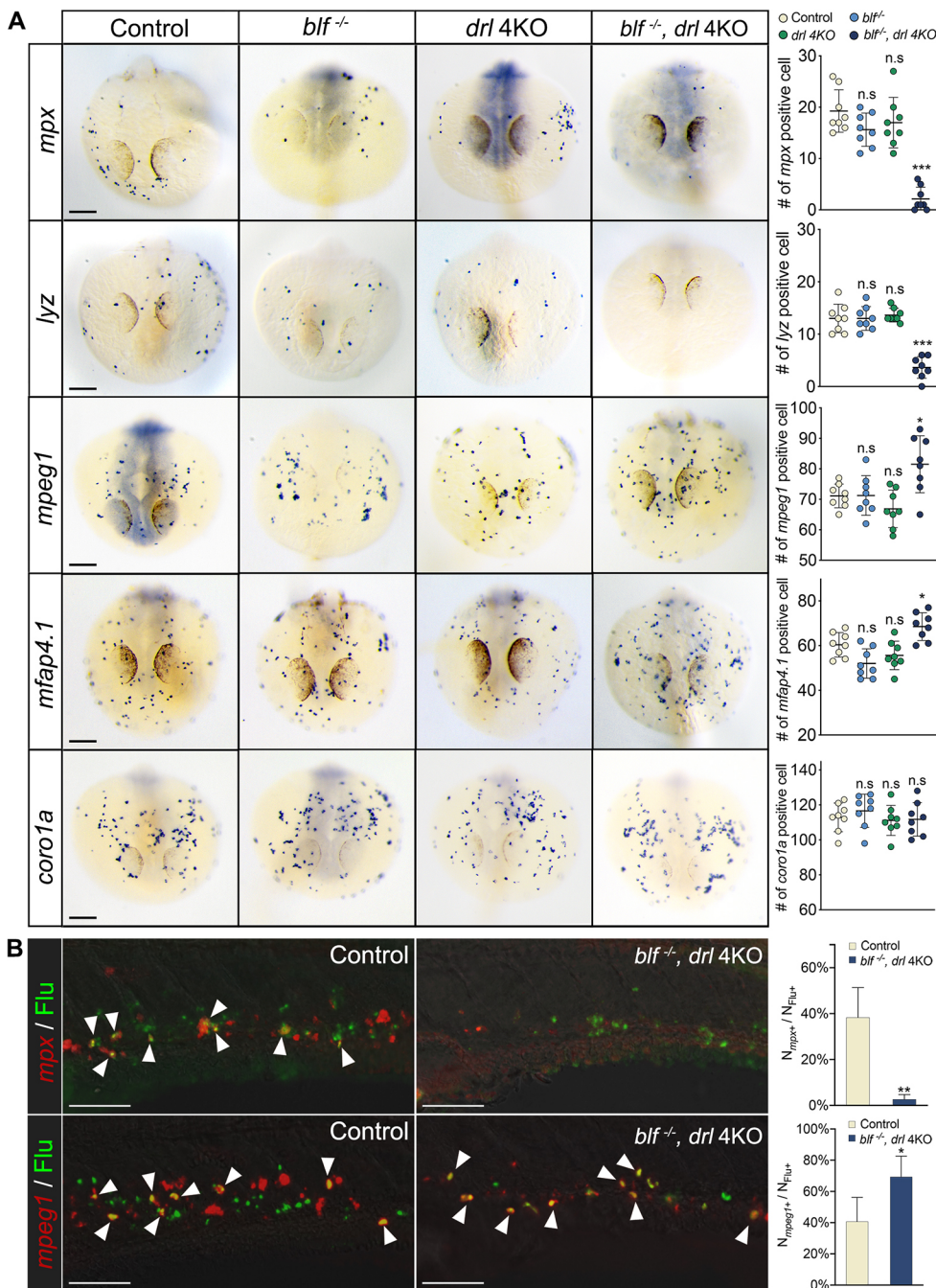


Fig. 4. *blf* and the *drl* cluster regulate macrophage versus neutrophil fate choice during primitive myelopoiesis.

(A) Left: RNA *in situ* hybridization of *mpx*, *lyz*, *mpeg1*, *mfp4.1* and *coro1a* expression at 23 hpf. Right: The number of myeloid cells in different genotypes for each marker. Scale bars: 100 μ m. (B) Left: Merged confocal images of the uncaged fluorescein and FISH signals in the trunk at 72 hpf. Scale bars: 50 μ m. White arrowheads indicate the overlapping of fluorescein and FISH staining. Right: Quantification of fluorescein-labeled myeloid cells adopting the neutrophil or macrophage fate in control and *blf*^{-/-}; *drl* 4KO embryos. N_{mpx+} , number of *mpx*-expressing cells; N_{mpeg1+} , number of *mpeg1*-expressing cells; N_{Flu+} , number of fluorescein-labeled cells. Quantification was carried out on a 150 μ m \times 275 μ m field. Data were collected for 12-16 embryos per experiment group. n.s., not significant, * P <0.05, ** P <0.01, *** P <0.001 (*t*-test).

action of Drl, we integrated the *blf*^{-/-}; *drl* 4KO RNA-seq and Drl CUT&Tag results with the binding and expression target analysis (BETA) pipeline (Wang et al., 2013). This showed that 1547 genes (Table S3) were directly regulated by Drl; the genes repressed by Drl showed higher regulatory potential scores than those that were activated, indicating that Drl mainly acts as a transcriptional repressor (Fig. 6E). GO analysis showed that genes repressed by Drl were enriched in processes such as vasculature development and myeloid leukocyte differentiation (Fig. 6F). CUT&Tag detected Drl situated at transcription regulatory regions of vasculogenesis-promoting genes, such as *etsrp*, *fli1rs* and *aplnra* as well as of monocytopenia-promoting genes, such as *irf8*, *irf5* and *bcl6ab* (Fig. 6G,H, Fig. S13). WISH results showed ectopic expression of *etsrp*, an essential regulator of vasculogenesis, in the intermediate

cell mass, and expression of *irf8*, a master driver of monocytopenia, was profoundly upregulated in the rostral blood island in *blf*^{-/-}; *drl* 4KO embryos (Figs 5D, 6G,H). To verify the transcription regulatory role of Drl on these genes, we overexpressed Drl in wild-type embryos by mRNA injection, and found a significant decrease in *irf8* and *etsrp* expression (Fig. 6G, H). To examine whether the mis-regulated *irf8* expression underpinned skewed myeloid lineage development, we employed knockdown of *irf8* by morpholino injection in *blf*^{-/-}; *drl* 4KO embryos and observed partially restored expression of the neutrophil marker gene *mpx* (Fig. 6I).

In summary, these results indicate that *blf* and *drl* cluster genes play dual roles in establishing normal transcription programs in different hematopoietic progenitors. In the intermediate cell mass,

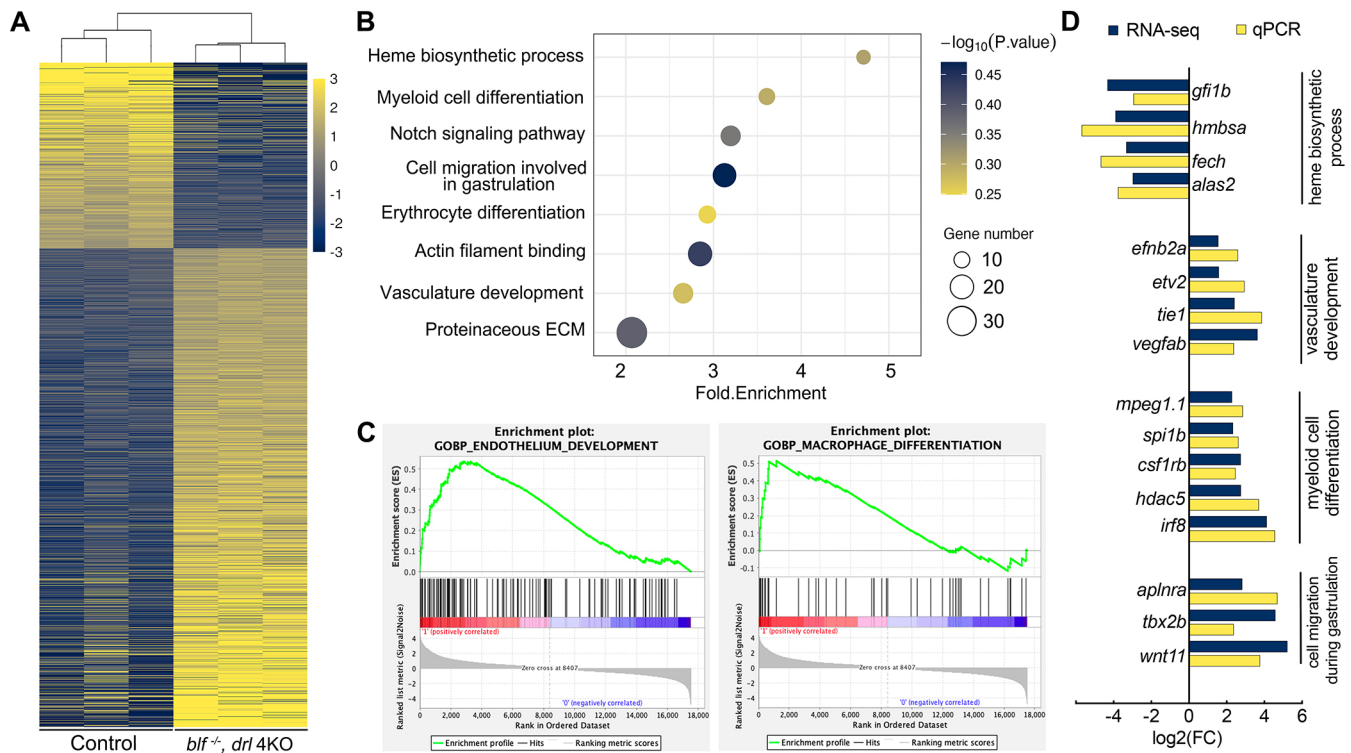


Fig. 5. *blf* and the *drl* cluster play essential roles in establishing a normal transcription program during primitive erythropoiesis and myelopoiesis.

(A) Heat map representation of genes differentially expressed in *blf*^{-/-}; *drl* 4KO hematopoietic progenitors at 22 hpf. Yellow, upregulated; blue, downregulated; gray, no significant change. (B) Bubble plot showing GO enrichment of differentially expressed genes in *blf*^{-/-}; *drl* 4KO hematopoietic progenitors. The size of the dots represents the number of differentially expressed genes in the corresponding biological process or molecular function. (C) Exemplary plots of significantly enriched pathways derived from GSEA. Criteria values for selection were enrichment score, family-wise error rate (P -value) <0.025 and FDR <0.05 . (D) Comparison of changes in expression of selected genes measured by RNA-seq and qPCR.

blf and *drl* cluster genes support the hematopoietic fate by constraining expression of vasculogenesis-promoting genes; in the rostral blood island, these genes sustain granulopoiesis by confining monocytopenia-promoting genes.

Zfp932 is a potential mammalian functional ortholog to the zebrafish *blf* and *drl* cluster genes

Given the conservation of the hematopoietic regulatory program in different vertebrates (Jagannathan-Bogdan and Zon, 2013), we speculated that mammalian functional ortholog(s) exist. We first deployed synteny analysis on both *blf* and *drl* cluster loci, but low synteny conservation (Fig. S14) prevented us from inferring orthologs by gene neighborhood. Multiple sequential C2H2 zinc fingers in the Blf and Drl cluster proteins presented a challenge in identifying orthologous genes with routine sequence similarity-based methods such as BLASTp. Therefore, we adopted a more sensitive, hidden Markov model (HMM)-based search method, HHpred, which is able to establish connections in remotely homologous, characterized proteins (Gabler et al., 2020). By conducting an iterative search with the Drl protein sequence against the human and mouse proteomes, a list of ortholog candidates was compiled. To screen the mammalian functional orthologs of zebrafish *blf* and *drl* cluster genes, mRNAs of the top 25 candidate genes on this list (Table S4), ranked by secondary structure scores, were prepared and microinjected into *blf*^{-/-}; *drl* 4KO embryos. Rescue efficacy was measured by mRNA levels of *hbae1* and *mpx*. Among all the candidate genes tested, Zfp932 was able to partially restore erythropoiesis and granulopoiesis in *blf*^{-/-}; *drl* 4KO embryos (Fig. 7, Fig. S15), which indicated that Zfp932 is a

potential mammalian functional ortholog to the zebrafish *blf* and *drl* cluster genes.

DISCUSSION

Lineage commitment of hematopoietic progenitor cells is governed by intricate gene regulatory networks. In the present study, we have presented *in vivo* evidence demonstrating that *blf* and *drl* cluster genes are important components of these programs. Our data revealed that *blf* and *drl* cluster genes act as crucial determinants of primitive erythropoiesis and myelopoiesis by constraining the expression of vasculogenesis-promoting and monocytopenia-promoting genes in two progenitor populations. The identification of these master regulators of hematopoietic fate enhances our understanding on this topic and may lead to improved strategies for the generation of hematopoietic cells *in vivo* and *in vitro* for regenerative medicine.

Besides defects of primitive hematopoiesis, our study shows that simultaneous loss of *blf* and *drl* cluster genes leads to disruption of HSC development and premature death at a juvenile stage. These results indicated that *blf* and *drl* cluster genes are also involved in definitive hematopoiesis. It is possible that *blf* and *drl* cluster genes act by a similar mechanism in definitive hematopoiesis: repressing endothelial genes to facilitate formation of HSCs. Further investigation is required to explore this possibility. We also observed that approximately 30% of *blf*^{-/-}; *drl* 4KO homozygous mutants were able to survive to adulthood and that these animals displayed mild anemia and nearly normal red blood cell differentiation. It would be interesting to examine how hematopoietic stem cells emerge in these ‘escapers’ and whether myeloid lineage cells form normally.

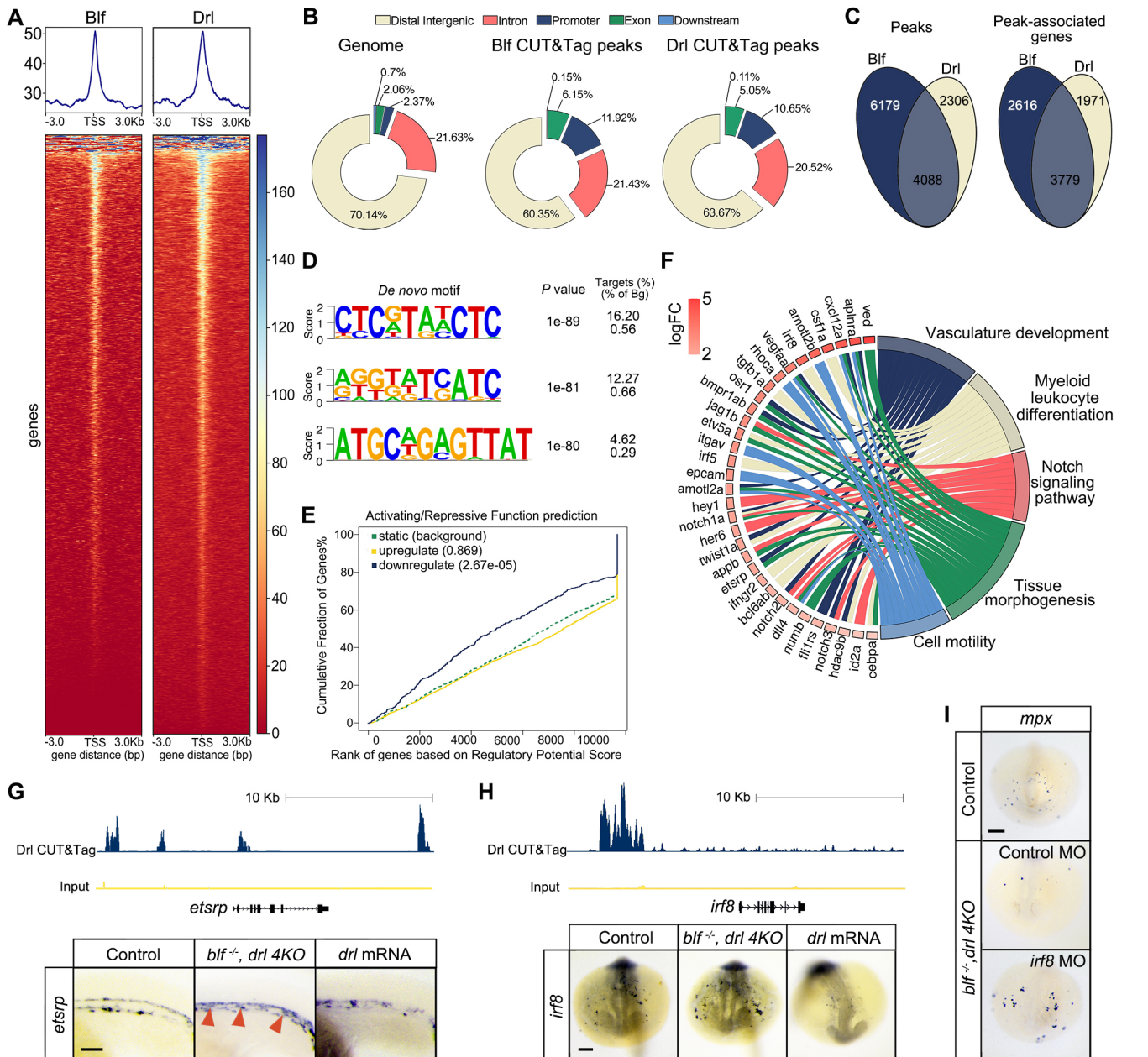


Fig. 6. *bif* and *drl* cluster genes restrict the expression of vasculogenesis- and monocytopenia-promoting genes. (A) Read densities and signal distribution heatmap of Bif and Drl CUT&Tag sequencing at gene-coding regions, with 3 kb upstream and 3 kb downstream of transcription start site (TSS) shown. (B) Genome-wide distribution of Bif and Drl CUT&Tag sequencing peaks. Promoter regions are defined as sequences within 3 kb of the TSS of annotated genes. Downstream regions are defined as sequences within 3 kb of the gene end. (C) Quantitative Venn diagram showing overlapping peaks and peak-associated genes between Bif and Drl in hematopoietic progenitors at 20 hpf. (D) *De novo* motif prediction on Drl-binding sites was performed on CUT&Tag data using HOMER. The top three motifs are shown. (E) Activating and repressive function prediction of Drl in hematopoietic progenitors. BETA software was used with default parameters (peaks within ± 100 kb of TSS) to integrate Drl CUT&Tag binding sites with expression data from the RNA-seq profile in hematopoietic progenitors from control and *bif*^{-/-}; *drl* 4KO animals ($n=3$). The yellow, blue and green lines represent genes activated, repressed or unaffected by Drl, respectively. The percentage of genes is cumulated by the rank of genes based on their regulatory potential scores. *P*-values (in parentheses) were derived from Kolmogorov–Smirnov tests. (F) Circular plot of 33 representative Drl direct target genes, simultaneously presenting a detailed view of the relationships between expression changes (left semicircle perimeter) and processes (right semicircle perimeter). Color code represents the log₂(fold change) value. (G) Top: Drl CUT&Tag binding profiles at the *etsrp* locus. Bottom: RNA *in situ* hybridization of *etsrp* expression in control ($n=37$), *bif*^{-/-}; *drl* 4KO ($n=36$) and *drl* overexpressing ($n=30$) embryos at the 22-somite stage; lateral view. Red arrowheads indicate ectopic *etsrp* expression in the intermediate cell mass. (H) Top: Drl CUT&Tag binding profiles at the *irf8* locus. Bottom: RNA *in situ* hybridization of *irf8* expression in control ($n=25$), *bif*^{-/-}; *drl* 4KO ($n=37$) and *drl* overexpressing ($n=36$) embryos at the 22-somite stage; frontal view. (I) RNA *in situ* hybridization of *mpx* expression in control ($n=34$) and *bif*^{-/-}; *drl* 4KO embryos injected with control ($n=26$) or *irf8* morpholino ($n=30$). Samples were collected at the 22-somite stage and are displayed as frontal view. Scale bars: 100 μ m.

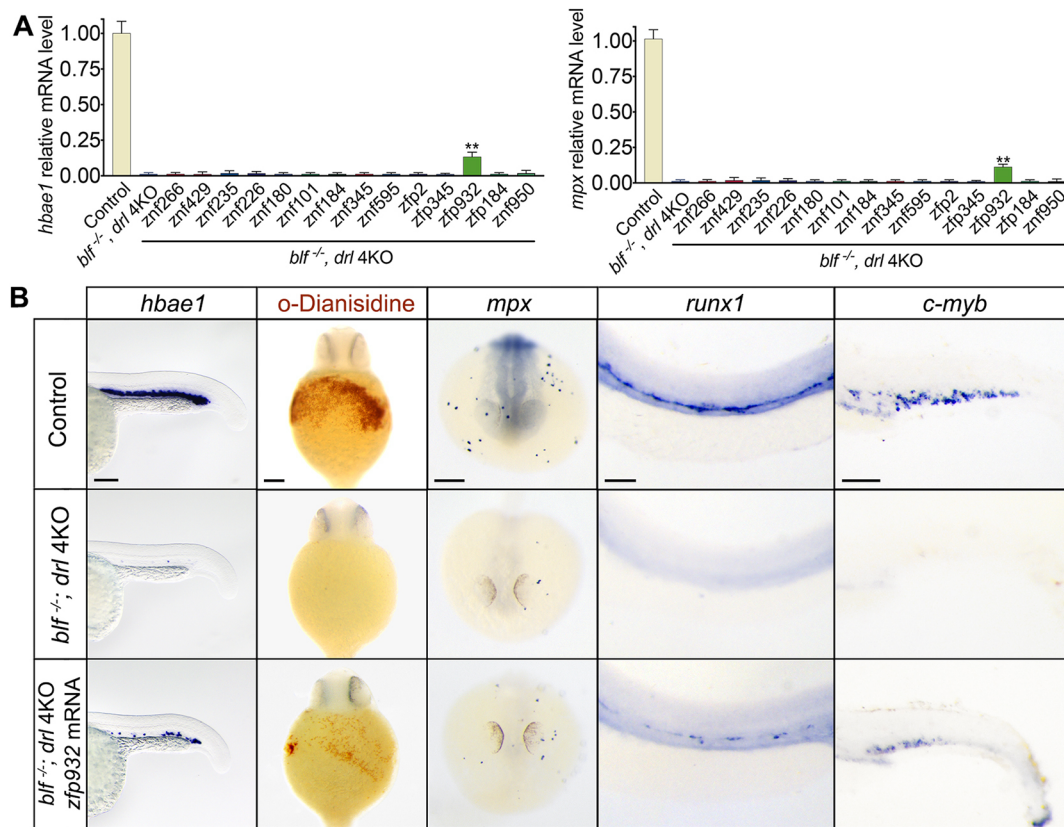


Fig. 7. Zfp932 is a potential mammalian functional ortholog of the zebrafish *blf* and *drl* cluster genes. (A) qPCR of the erythroid marker gene *hbae1* and the neutrophil marker gene *mpk* in *blf*^{-/-}; *drl* 4KO embryos after injection of human or mouse mRNA. Data are mean±s.e.m. of at least three replicates. ***P*<0.01. (B) Left: Expression of *hbae1* in 23 hpf embryos; *n*=27, 32 and 29 for each experimental set. Middle: Whole-mount o-dianisidine staining of 36 hpf embryos; *n*=31, 39 and 33 for each experimental set. Ventral views. Right three panels: RNA *in situ* hybridization of *mpk*, *runx1* and *c-myb* expression. For *mpk* WISH, *n*=38, 33 and 25. For *runx1* WISH, *n*=38, 29 and 30. For *c-myb* WISH, *n*=31, 25 and 37. Listed sample sizes relate to each group shown from top to bottom. Scale bars: 100 μm.

Intriguingly, our data indicated that *blf* and *drl* cluster genes play multifunctional roles in hematopoiesis by binding to gene regulatory regions of key endothelial and hematopoietic factors. These different roles may require a variety of partners and future studies will be needed to identify specific partners in different cell populations. Given that long-tandem, zinc-finger arrays may be functionally broken into several regions of fewer zinc-finger repeats (Emerson and Thomas, 2009), it is possible that *blf* and *drl* cluster factors bind a variety of motifs as a result of interacting with distinct partners.

In a previous study, Pimtong et al. reported that knockdown of the expression of *drl3* with morpholino injection could cause decreased primitive erythropoiesis and myelopoiesis (Pimtong et al., 2014). We also observed a mild erythropoiesis defect in *drl* 4KO embryos (Fig. 1A,B), indicating that *drl* cluster genes probably act in a dosage-dependent fashion. During the process of generating the *drl* 4KO allele, we also obtained two CRISPR alleles bearing mutants on *drl3*; no overt hematopoietic defects were observed in the homozygous embryos of these alleles.

By means of rescue screening, we identified Zfp932 as a potential mammalian functional equivalent to *blf* and *drl* cluster genes. This suggested that the mechanisms of hematopoietic cell fate commitment, discussed in the current study, may be conserved during evolution. Interestingly, repeated sequence motif scanning with RADAR (Heger and Holm, 2000) identified multiple CDQCGK motifs on *Drl*, *Blf* and *Zfp932* sequences (Fig. S16). This suggested that they represent a subgroup of zinc-finger proteins

and it will be of great interest to characterize the biochemical properties and functions of this motif.

Previous reports demonstrated that *etsrp* is a potent positive regulator of endothelial development in zebrafish (Sumanas and Lin, 2006; Liu and Patient, 2008), but ectopic expression of *etsrp* in the intermediate cell mass did not induce excess endothelialization in *blf*^{-/-}; *drl* 4KO homozygous embryos (Fig. 6G). One possible explanation for this observation is that the differentiation of hemangioblasts to hematopoietic cells is suspended, and that immature hemangioblasts possessing endothelial characteristics went into apoptosis.

MATERIALS AND METHODS

Animals

All animal experiments were carried out in accordance with the approved guidelines of the Institutional Animal Care and Use Committee of the Nanjing University. All zebrafish lines were kept on the AB background.

RNA *in situ* hybridization

Transcription of digoxigenin-labeled antisense RNA probes was performed using standard methods. WISH was carried out as previously described (Thisse and Thisse, 2008).

Generation of *drl* cluster knockout zebrafish

gRNAs were designed using a CRISPR/Cas9 target online predictor (<https://cctop.cos.uni-heidelberg.de>), and 50 pg of sgRNAs and 500 pg of Cas9

protein were co-injected into one-cell-stage embryos. Live embryo genotyping was carried out as previously described (Zhang et al., 2020) and one allele bearing a 49,188 bp deletion on the *drl* cluster was identified and used for subsequent experiments. Genotyping oligos used were: *drl* 4KO allele: 5'-GAAACTCAGAAAGGTTTGAACAACCC-3' and 5'-CTGAGTTCAACAATCGAAGCATATTAACCAACCAG-3'; *drl* cluster WT allele#1: 5'-GGACCGAGTATCAGTAGTATGCA-3' and 5'-GTTAG-CTGGTACCCACTTCTC-3'; *drl* cluster WT allele#2: 5'-GGTGTCTGAG-GATGCACGAC-3' and 5'-AAAGCAGAGAATTGTTAACCAGG-3'.

Histochemistry

Based on a previously described protocol (Paffett-Lugassy and Zon, 2005), o-dianisidine staining was used to detect the presence of hemoglobin. Embryos were stained in the dark for 30 min at room temperature with a solution containing o-dianisidine (0.6 mg/ml), 0.01 M sodium acetate (pH 4.5), 0.65% H₂O₂ and 40% (vol/vol) ethanol. Once stained, embryos were washed with RO water and then fixed in 4% paraformaldehyde for at least 1 h at room temperature. Pigments were removed from fixed embryos by incubating in a solution of 0.8% KOH, 0.9% H₂O₂ and 0.1% Tween-20 for 30 min at room temperature. Based on previously described protocols (Le Guyader et al., 2008), Sudan Black (SB; Sigma-Aldrich) solution was used to treat the paraformaldehyde-fixed embryos for 20 min, washed extensively in 70% ethanol in water, then progressively rehydrated in PBS and 0.1% Tween-20 (PBT).

Quantitative real-time PCR

Total RNA was prepared using TRIzol (Invitrogen, 15596) and Direct-zol RNA Miniprep (Zymo Research, R2052). cDNA was synthesized with the PrimerScript RT kit (Takara Bio, RR047A). RT-qPCR reactions were performed on the Roche LightCycler system using the SYBR Green Master Mix (Takara Bio, RR420A). Melt curves were examined to ensure primer specificity. Primers used in RT-qPCR were designed to span exon-exon junctions and are listed in Table S5.

TUNEL assay

For TUNEL reactions, staining with anti-digoxigenin-fluorescein was performed according to the manual of In Situ Cell Death Detection Kit (Sigma-Aldrich, 11684795910). The samples were fixed for 4 h in 4% paraformaldehyde, then washed twice, 10 min each wash, in PBS. After washing in PBS, DNA breaks were elongated with terminal transferase and digoxigenin-dUTP solution.

Imaging

Whole-mount imaging was performed using a Leica DFC320 camera on a Leica M205FA stereomicroscope. All confocal images were acquired using a Zeiss LSM880 confocal microscope.

Survival curve

At 7 dpf, 80 wild-type siblings and *blf*^{-/-}; *drl* 4KO animals were each put into a 3 l tank. Every 3 days, the number of living fish was counted until 60 dpf. A Kaplan–Meier curve was generated using Prism 7 (GraphPad) (Goel et al., 2010).

Laser-activated cell labeling

Lineage tracking was performed as described previously (Jin et al., 2007). Briefly, CMNB-caged-fluorescein (Invitrogen, F7103) was injected into one-cell-stage embryos then left to develop in the dark. At the 22-somite stage, cells at the anterior hematopoietic site were uncaged by focusing and confining 405-nm laser excitation. Successful activation of fluorescein was verified by local enhancement of green fluorescence. Uncaged embryos were incubated in the dark until fixation at 72 hpf for further analysis.

Two-color fluorescence staining

Two-color fluorescence staining was performed essentially as described previously (Jin et al., 2006). Briefly, embryos were first hybridized with a digoxigenin-labeled antisense RNA probe then incubated overnight with anti-fluorescein-POD, Fab fragments (Roche, 11426346910) and detected with

Alexa Fluor 488 tyramide substrate (Invitrogen, B40953). The color reaction was then stopped by sequential washing with methanol/PBS Tween-20 (PBST) and 1% H₂O₂/methanol. Finally, the embryos were subjected to a second color staining with anti-digoxigenin-POD, Fab fragments (Roche, 11207733910) and Alexa Fluor 555 tyramide (Invitrogen, B40955) as a substrate.

Transcriptome sequencing

The libraries were constructed with the NEBNext Single Cell/Low Input RNA Library Prep Kit for Illumina (NEB, 6420) and sequenced on the Illumina NovaSeq platform. HISAT2 V2.1.0 was used to map the sample sequencing reads to the GRCz11 reference genome. Gene expression counts were calculated using FeatureCounts v1.6.0. based on current Ensemble annotation. The R package DESeq2 was then employed to make differential gene expression calls.

CUT&Tag sequencing

CUT&Tag was performed in two biological replicates as originally described (Kaya-Okur et al., 2020) with the Hyperactive Universal CUT&Tag Assay Kit for Illumina (Vazyme, TD-903). Briefly, mRNA was injected into embryos at the one-cell stage, and RFP⁺ hematopoietic progenitors were collected by FACS at 20 hpf then immobilized on Concanavalin A-coated paramagnetic beads and permeabilized with digitonin. Cells were incubated overnight with the anti-FLAG antibody (Sigma-Aldrich, F3165). To increase the number of Protein A/G binding sites for each bound antibody, goat anti-mouse IgG H&L antibody (Abcam, ab6708) was incubated at room temperature for 1 h. Tethered cells were washed thoroughly to remove unbound antibody, and then incubated with pAG-Tn5 for 60 min. Tn5 transposase-mediated tagmentation was then initiated by the addition of MgCl₂. Tagmented DNA was extracted using magnetic beads then sequencing libraries were generated as previously described (Kaya-Okur et al., 2020), and sequenced on an Illumina HiSeq 2500 platform. *Drl*- and *Blf*-binding regions were identified by model-based analysis of ChIP-seq (MACS) (Zhang et al., 2008) with the parameter 'macs2 callpeak -t C&T_flag.bam -c Input.bam -n C&T_flag_peaks -g 1.37e9 -f BAMPE -q 0.01'. The peaks were annotated using ChIPseeker (Yu et al., 2015). Each peak set was obtained by the intersection of two independent biological replicates.

Morpholino oligonucleotides

irf8 splicing morpholino oligonucleotides (MO)^{SP} (5'-AATGTTTCGCT-TACTTTGAAAATGG-3') were synthesized based on a previous report (Li et al., 2011). Standard control morpholino was purchased from Gene Tools. One-cell-stage embryos were injected with 2 nl of morpholino solution at a concentration of 0.6 mM *irf8* MO^{SP}.

Statistical analysis

Two-sided, unpaired Student's *t*-tests were performed using GraphPad Prism 7 software and numerical data are presented as mean±s.e.m. Differences were considered significant if the probability value was *P*<0.05 and highly significant if the probability value was *P*<0.01. All experiments were carried out with at least three biological replicates. The numbers of animals used are described in the corresponding figure legends.

Acknowledgements

We thank all members of the Lou lab for valuable insight and suggestions. We also thank Dr Min Li from core facilities of Nanjing University for technical support.

Competing interests

The authors declare no competing or financial interests.

Author contributions

Conceptualization: X.L.; Methodology: Y.Y.; Formal analysis: X.Z., Y.Y., Y.W.; Investigation: X.Z., Y.Y., Y.W., X.L.; Data curation: Y.Y.; Writing - original draft: X.L.; Supervision: Q.Z., X.L.; Project administration: X.L.; Funding acquisition: Q.Z., X.L.

Funding

This research was undertaken, in part, thanks to grant funding from National Natural Science Foundation of China (NSFC 31970765 to X.L. and NSFC 31970769 to Q.Z.).

Data availability

RNA-seq and CUT&Tag data have been deposited in the NCBI Gene Expression Omnibus under accession numbers GSE202193 and GSE212060, respectively.

Peer review history

The peer review history is available online at <https://journals.biologists.com/dev/lookup/doi/10.1242/dev.200919.reviewer-comments.pdf>

References

- Bertrand, J. Y., Kim, A. D., Violette, E. P., Stachura, D. L., Cisson, J. L. and Traver, D. (2007). Definitive hematopoiesis initiates through a committed erythromyeloid progenitor in the zebrafish embryo. *Development* **134**, 4147-4156. doi:10.1242/dev.012385
- Carroll, K. J. and North, T. E. (2014). Oceans of opportunity: exploring vertebrate hematopoiesis in zebrafish. *Exp. Hematol.* **42**, 684-696. doi:10.1016/j.exphem.2014.05.002
- Da'as, S. I., Coombs, A. J., Balci, T. B., Grondin, C. A., Ferrando, A. A. and Berman, J. N. (2012). The zebrafish reveals dependence of the mast cell lineage on Notch signaling in vivo. *Blood* **119**, 3585-3594. doi:10.1182/blood-2011-10-385989
- Dahl, R., Walsh, J. C., Lancki, D., Laslo, P., Iyer, S. R., Singh, H. and Simon, M. C. (2003). Regulation of macrophage and neutrophil cell fates by the PU.1:C/EBP α ratio and granulocyte colony-stimulating factor. *Nat. Immunol.* **4**, 1029-1036. doi:10.1038/ni973
- Davidson, A. J. and Zon, L. I. (2004). The 'definitive' (and 'primitive') guide to zebrafish hematopoiesis. *Oncogene* **23**, 7233-7246. doi:10.1038/sj.onc.1207943
- De Bruijn, M. (2014). The hemangioblast revisited. *Blood* **124**, 2472-2473. doi:10.1182/blood-2014-09-597674
- De Bruijn, M. F., Ma, X., Robin, C., Ottersbach, K., Sanchez, M. J. and Dzierzak, E. (2002). Hematopoietic stem cells localize to the endothelial cell layer in the midgestation mouse aorta. *Immunity* **16**, 673-683. doi:10.1016/S1074-7613(02)00313-8
- Dzierzak, E. and Bigas, A. (2018). Blood development: hematopoietic stem cell dependence and independence. *Cell Stem Cell* **22**, 639-651. doi:10.1016/j.stem.2018.04.015
- Elsaid, R., Soares-Da-Silva, F., Peixoto, M., Amiri, D., Mackowski, N., Pereira, P., Bandeira, A. and Cumano, A. (2020). Hematopoiesis: a layered organization across chordate species. *Front. Cell Dev. Biol.* **8**, 606642. doi:10.3389/fcell.2020.606642
- Emerson, R. O. and Thomas, J. H. (2009). Adaptive evolution in zinc finger transcription factors. *PLoS Genet.* **5**, e1000325. doi:10.1371/journal.pgen.1000325
- Gabler, F., Nam, S. Z., Till, S., Mirdita, M., Steinegger, M., Soding, J., Lupas, A. N. and Alva, V. (2020). Protein sequence analysis using the MPI bioinformatics toolkit. *Curr. Protoc. Bioinform.* **72**, e108. doi:10.1002/cpbi.108
- Goel, M. K., Khanna, P. and Kishore, J. (2010). Understanding survival analysis: Kaplan-Meier estimate. *Int. J. Ayurveda Res.* **1**, 274-278. doi:10.4103/0974-7788.76794
- Gomez Perdiguero, E., Klapproth, K., Schulz, C., Busch, K., Azzoni, E., Crozet, L., Garner, H., Trouillet, C., De Bruijn, M. F., Geissmann, F. et al. (2015). Tissue-resident macrophages originate from yolk-sac-derived erythromyeloid progenitors. *Nature* **518**, 547-551. doi:10.1038/nature13989
- Heger, A. and Holm, L. (2000). Rapid automatic detection and alignment of repeats in protein sequences. *Proteins* **41**, 224-237. doi:10.1002/1097-0134(20001101)41:2<224::AID-PROT70>3.0.CO;2-Z
- Herbomel, P., Thisse, B. and Thisse, C. (1999). Ontogeny and behaviour of early macrophages in the zebrafish embryo. *Development* **126**, 3735-3745. doi:10.1242/dev.126.17.3735
- Hou, N., Yang, Y., Scott, I. C. and Lou, X. (2017). The Sec domain protein Scfd1 facilitates trafficking of ECM components during chondrogenesis. *Dev. Biol.* **421**, 8-15. doi:10.1016/j.ydbio.2016.11.010
- Huber, T. L., Kouskoff, V., Fehling, H. J., Palis, J. and Keller, G. (2004). Haemangioblast commitment is initiated in the primitive streak of the mouse embryo. *Nature* **432**, 625-630. doi:10.1038/nature03122
- Jagannathan-Bogdan, M. and Zon, L. I. (2013). Hematopoiesis. *Development* **140**, 2463-2467. doi:10.1242/dev.083147
- Jin, H., Xu, J. and Wen, Z. (2007). Migratory path of definitive hematopoietic stem/progenitor cells during zebrafish development. *Blood* **109**, 5208-5214. doi:10.1182/blood-2007-01-069005
- Jin, H., Xu, J., Qian, F., Du, L., Tan, C. Y., Lin, Z., Peng, J. and Wen, Z. (2006). The 5' zebrafish scl promoter targets transcription to the brain, spinal cord, and hematopoietic and endothelial progenitors. *Dev. Dyn.* **235**, 60-67. doi:10.1002/dvdy.20613
- Jin, H., Li, L., Xu, J., Zhen, F., Zhu, L., Liu, P. P., Zhang, M., Zhang, W. and Wen, Z. (2012). Runx1 regulates embryonic myeloid fate choice in zebrafish through a negative feedback loop inhibiting Pu.1 expression. *Blood* **119**, 5239-5249. doi:10.1182/blood-2011-12-398362
- Kaya-Okur, H. S., Janssens, D. H., Henikoff, J. G., Ahmad, K. and Henikoff, S. (2020). Efficient low-cost chromatin profiling with CUT&Tag. *Nat. Protoc.* **15**, 3264-3283. doi:10.1038/s41596-020-0373-x
- Kobayashi, I., Kobayashi-Sun, J., Hirakawa, Y., Ouchi, M., Yasuda, K., Kamei, H., Fukuhara, S. and Yamaguchi, M. (2020). Dual role of Jam3b in early hematopoietic and vascular development. *Development* **147**, dev181040. doi:10.1242/dev.181040
- Lancrin, C., Sroczynska, P., Stephenson, C., Allen, T., Kouskoff, V. and Lacaud, G. (2009). The haemangioblast generates hematopoietic cells through a haemogenic endothelium stage. *Nature* **457**, 892-895. doi:10.1038/nature07679
- Lavin, Y., Mortha, A., Rahman, A. and Merad, M. (2015). Regulation of macrophage development and function in peripheral tissues. *Nat. Rev. Immunol.* **15**, 731-744. doi:10.1038/nri3920
- Le Guyader, D., Redd, M. J., Colucci-Guyon, E., Murayama, E., Kissa, K., Briolat, V., Mordelet, E., Zapata, A., Shinomiya, H. and Herbomel, P. (2008). Origins and unconventional behavior of neutrophils in developing zebrafish. *Blood* **111**, 132-141. doi:10.1182/blood-2007-06-095398
- Li, L., Jin, H., Xu, J., Shi, Y. and Wen, Z. (2011). Irf8 regulates macrophage versus neutrophil fate during zebrafish primitive myelopoiesis. *Blood* **117**, 1359-1369. doi:10.1182/blood-2010-06-290700
- Li, L., Yan, B., Shi, Y. Q., Zhang, W. Q. and Wen, Z. L. (2012). Live imaging reveals differing roles of macrophages and neutrophils during zebrafish tail fin regeneration. *J. Biol. Chem.* **287**, 25353-25360. doi:10.1074/jbc.M112.349126
- Li, Y., Nakka, K., Olender, T., Gingras-Gelinas, P., Wong, M. M., Robinson, D. C. L., Bandukwala, H., Palii, C. G., Neyret, O., Brand, M. et al. (2021). Chromatin and transcription factor profiling in rare stem cell populations using CUT&Tag. *STAR Protoc.* **2**, 100751. doi:10.1016/j.xpro.2021.100751
- Liu, F. and Patient, R. (2008). Genome-wide analysis of the zebrafish ETS family identifies three genes required for hemangioblast differentiation or angiogenesis. *Circ. Res.* **103**, 1147-1154. doi:10.1161/CIRCRESAHA.108.179713
- Menegatti, S., De Kruijff, M., Garcia-Alegria, E., Lacaud, G. and Kouskoff, V. (2019). Transcriptional control of blood cell emergence. *FEBS Lett.* **593**, 3304-3315. doi:10.1002/1873-3468.13585
- Orkin, S. H. and Zon, L. I. (2008). Hematopoiesis: an evolving paradigm for stem cell biology. *Cell* **132**, 631-644. doi:10.1016/j.cell.2008.01.025
- Paffett-Lugassy, N. N. and Zon, L. I. (2005). Analysis of hematopoietic development in the zebrafish. *Methods Mol. Med.* **105**, 171-198. doi:10.1385/1-59259-826-9:171
- Pimanda, J. E., Ottersbach, K., Knezevic, K., Kinston, S., Chan, W. Y., Wilson, N. K., Landry, J. R., Wood, A. D., Kolb-Kokocinski, A., Green, A. R. et al. (2007). Gata2, Fli1, and Scl form a recursively wired gene-regulatory circuit during early hematopoietic development. *Proc. Natl. Acad. Sci. USA* **104**, 17692-17697. doi:10.1073/pnas.0707045104
- Pimpong, W., Datta, M., Ulrich, A. M. and Rhodes, J. (2014). Drl3 governs primitive hematopoiesis in zebrafish. *Sci. Rep.* **4**, 5791. doi:10.1038/srep05791
- Rosenbauer, F. and Tenen, D. G. (2007). Transcription factors in myeloid development: balancing differentiation with transformation. *Nat. Rev. Immunol.* **7**, 105-117. doi:10.1038/nri2024
- Sumanas, S. and Lin, S. (2006). Ets1-related protein is a key regulator of vasculogenesis in zebrafish. *PLoS Biol.* **4**, e10. doi:10.1371/journal.pbio.0040010
- Sumanas, S., Zhang, B., Dai, R. and Lin, S. (2005). 15-zinc finger protein Bloody Fingers is required for zebrafish morphogenetic movements during neurulation. *Dev. Biol.* **283**, 85-96. doi:10.1016/j.ydbio.2005.04.007
- Takeuchi, M., Fuse, Y., Watanabe, M., Andrea, C. S., Takeuchi, M., Nakajima, H., Ohashi, K., Kaneko, H., Kobayashi-Osaki, M., Yamamoto, M. et al. (2015). LSD1/KDM1A promotes hematopoietic commitment of hemangioblasts through downregulation of ETV2. *Proc. Natl. Acad. Sci. USA* **112**, 13922-13927. doi:10.1073/pnas.1517326112
- Thisse, C. and Thisse, B. (2008). High-resolution in situ hybridization to whole-mount zebrafish embryos. *Nat. Protoc.* **3**, 59-69. doi:10.1038/nprot.2007.514
- Vogeli, K. M., Jin, S. W., Martin, G. R. and Stainier, D. Y. (2006). A common progenitor for hematopoietic and endothelial lineages in the zebrafish gastrula. *Nature* **443**, 337-339. doi:10.1038/nature05045
- Wang, S., Sun, H., Ma, J., Zang, C., Wang, C., Wang, J., Tang, Q., Meyer, C. A., Zhang, Y. and Liu, X. S. (2013). Target analysis by integration of transcriptome and ChIP-seq data with BETA. *Nat. Protoc.* **8**, 2502-2515. doi:10.1038/nprot.2013.150
- Wang, L., Gao, S., Wang, H., Xue, C., Liu, X., Yuan, H., Wang, Z., Chen, S., Chen, Z., De The, H. et al. (2020). Interferon regulatory factor 2 binding protein 2b regulates neutrophil versus macrophage fate during zebrafish definitive myelopoiesis. *Haematologica* **105**, 325-337. doi:10.3324/haematol.2019.217596
- Watanabe, S., Alexander, M., Misharin, A. V. and Budinger, G. R. S. (2019). The role of macrophages in the resolution of inflammation. *J. Clin. Invest.* **129**, 2619-2628. doi:10.1172/JCI124615
- Wells, M. and Steiner, L. (2022). Epigenetic and transcriptional control of erythropoiesis. *Front. Genet.* **13**, 805265. doi:10.3389/fgene.2022.805265
- Wolfe, S. A., Nekudova, L. and Pabo, C. O. (2000). DNA recognition by Cys₂His₂ zinc finger proteins. *Annu. Rev. Biophys. Biomol. Struct.* **29**, 183-212. doi:10.1146/annurev.biophys.29.1.183
- Wu, Y. and Hirschi, K. K. (2020). Tissue-resident macrophage development and function. *Front. Cell Dev. Biol.* **8**, 617879. doi:10.3389/fcell.2020.617879
- Wynn, T. A. and Vannella, K. M. (2016). Macrophages in tissue repair, regeneration, and fibrosis. *Immunity* **44**, 450-462. doi:10.1016/j.immuni.2016.02.015

- Xu, J., Du, L. and Wen, Z.** (2012). Myelopoiesis during zebrafish early development. *J. Genet. Genomics* **39**, 435-442. doi:10.1016/j.jgg.2012.06.005
- Yu, G., Wang, L. G. and He, Q. Y.** (2015). ChIPseeker: an R/Bioconductor package for ChIP peak annotation, comparison and visualization. *Bioinformatics* **31**, 2382-2383. doi:10.1093/bioinformatics/btv145
- Zhang, Y., Liu, T., Meyer, C. A., Eeckhoute, J., Johnson, D. S., Bernstein, B. E., Nusbaum, C., Myers, R. M., Brown, M., Li, W. et al.** (2008). Model-based analysis of ChIP-Seq (MACS). *Genome Biol.* **9**, R137. doi:10.1186/gb-2008-9-9-r137
- Zhang, X., Zhang, Z., Zhao, Q. and Lou, X.** (2020). Rapid and efficient live zebrafish embryo genotyping. *Zebrafish* **17**, 56-58. doi:10.1089/zeb.2019.1796

Supplemental Figure 1

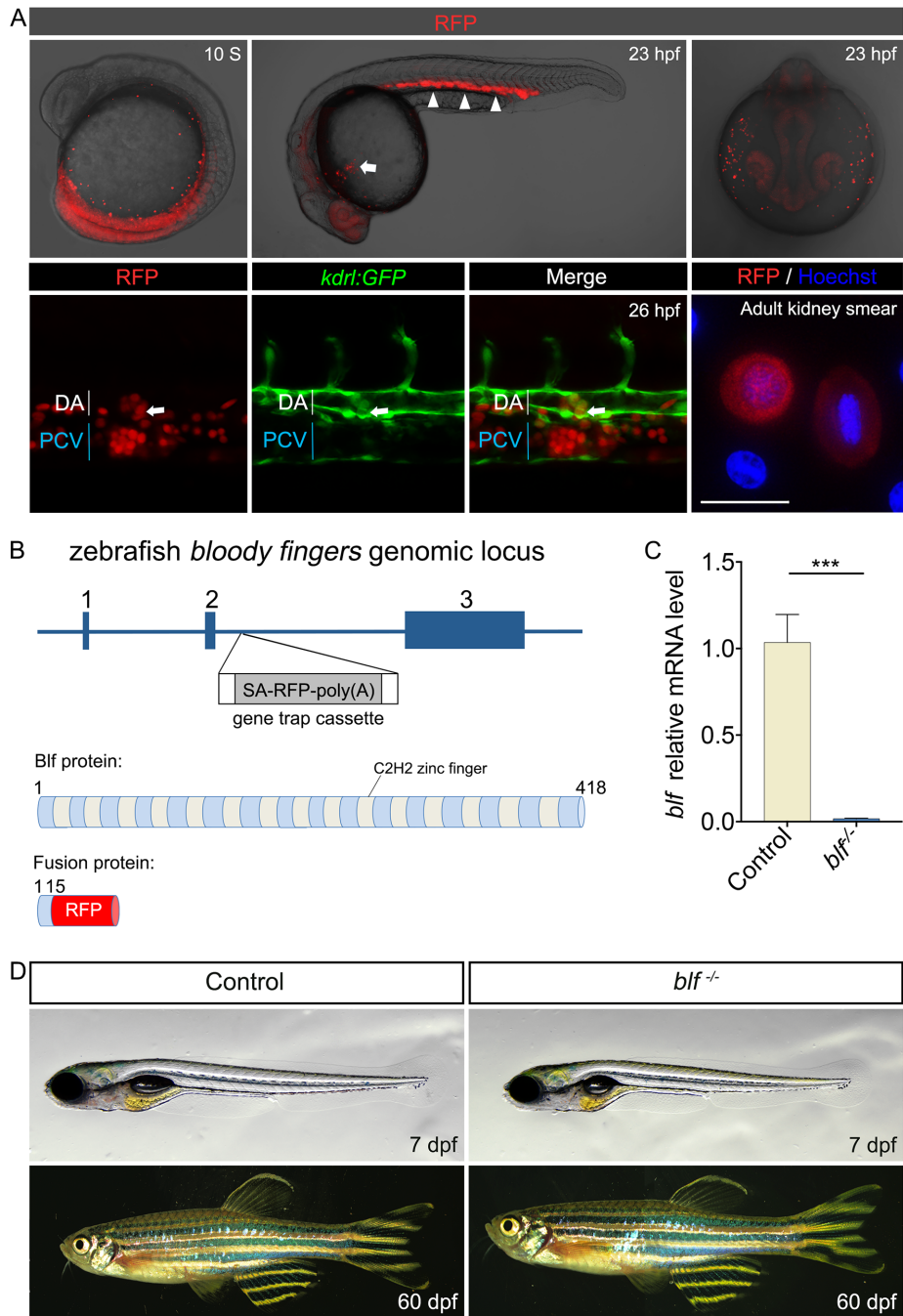


Fig. S1. Identification of the gene trapping line RP2-527. **(A)** RFP expression pattern in zebrafish gene trapping line RP2-527. At the 10 somite stage, RFP signal emerged in the bilateral stripes of the posterior lateral-plate mesoderm. Before circulation begins, RFP signal

could be observed in both the intermediate cell mass (white arrow) and the anterior hematopoietic site (white arrow). At 26 hpf, some RFP positive cells co-expressed the blood vessel endothelium reporter *flk1:GFP* and were indeed localized in the ventral side of dorsal aorta, demonstrating that these cells were hemogenic endothelial cells. In adult RP2-527 fish, an RFP signal could be observed in HSC-like cells in kidney. **(B)** Upper panel, the zebrafish *bfl* genomic locus. The transposon is inserted in the 2nd intron. Lower panel, schematic representations of the domain structure of the wild type zebrafish Blf protein and the fusion protein in RP2-527 fish. **(C)** QPCR results showing the absence of *bfl* mRNA in RP2-527 homozygous embryos. Data are mean \pm SEM of at least three replicates. *** $P < 0.001$. **(D)** Live images of control (wild type) and *bfl*^{-/-} animals at the designated time points. Lateral view with head to left.

Supplemental Figure 2

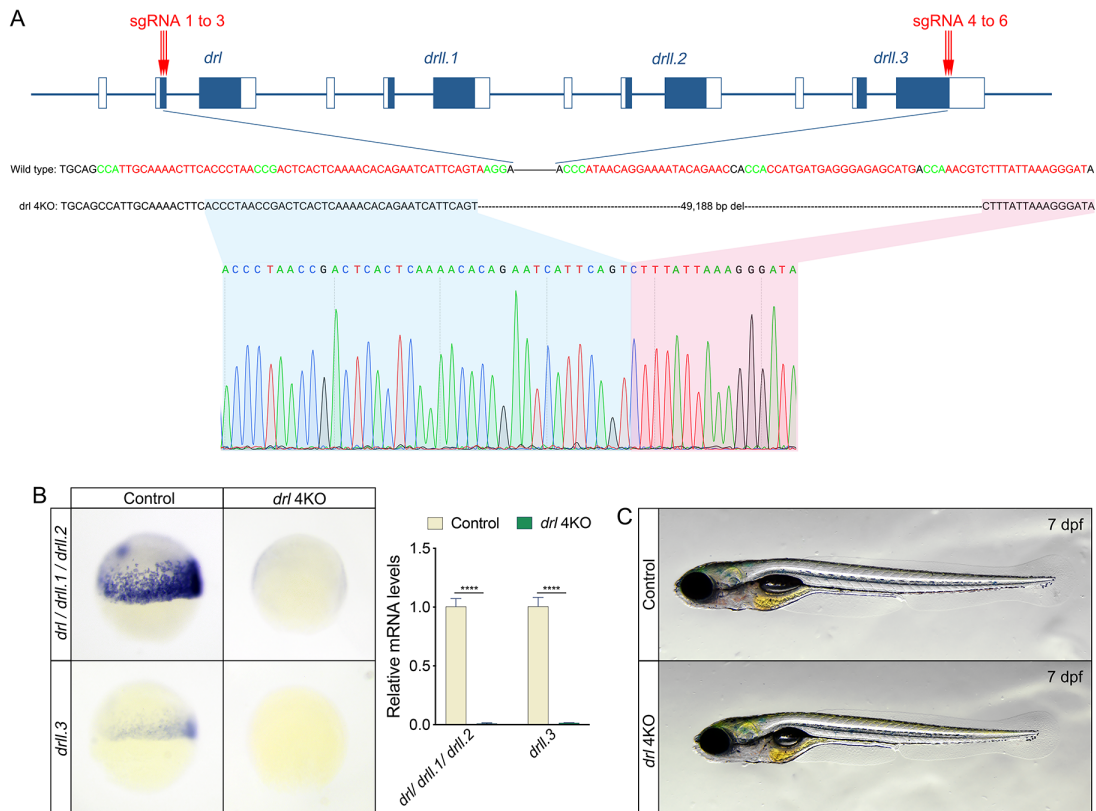


Fig. S2. Generation of *drl* cluster knockout zebrafish line. **(A)** Upper panel, the zebrafish *drl* cluster genomic locus and Cas9/sgRNA targeting sites. Lower panel, Sanger sequencing of genotyping PCR products indicating the 49,188 bp deletion on the *drl* cluster locus. **(B)** Whole mount *in situ* hybridization and qPCR results showing the absence of *drl* cluster genes mRNA in *drl* 4KO embryos. Data are mean \pm SEM of at least three replicates. **** $P < 0.0001$. **(C)** Live images of control (wild type) and *drl* 4KO fish at 7 days post fertilization. Lateral view with head to left.

Supplemental Figure 3

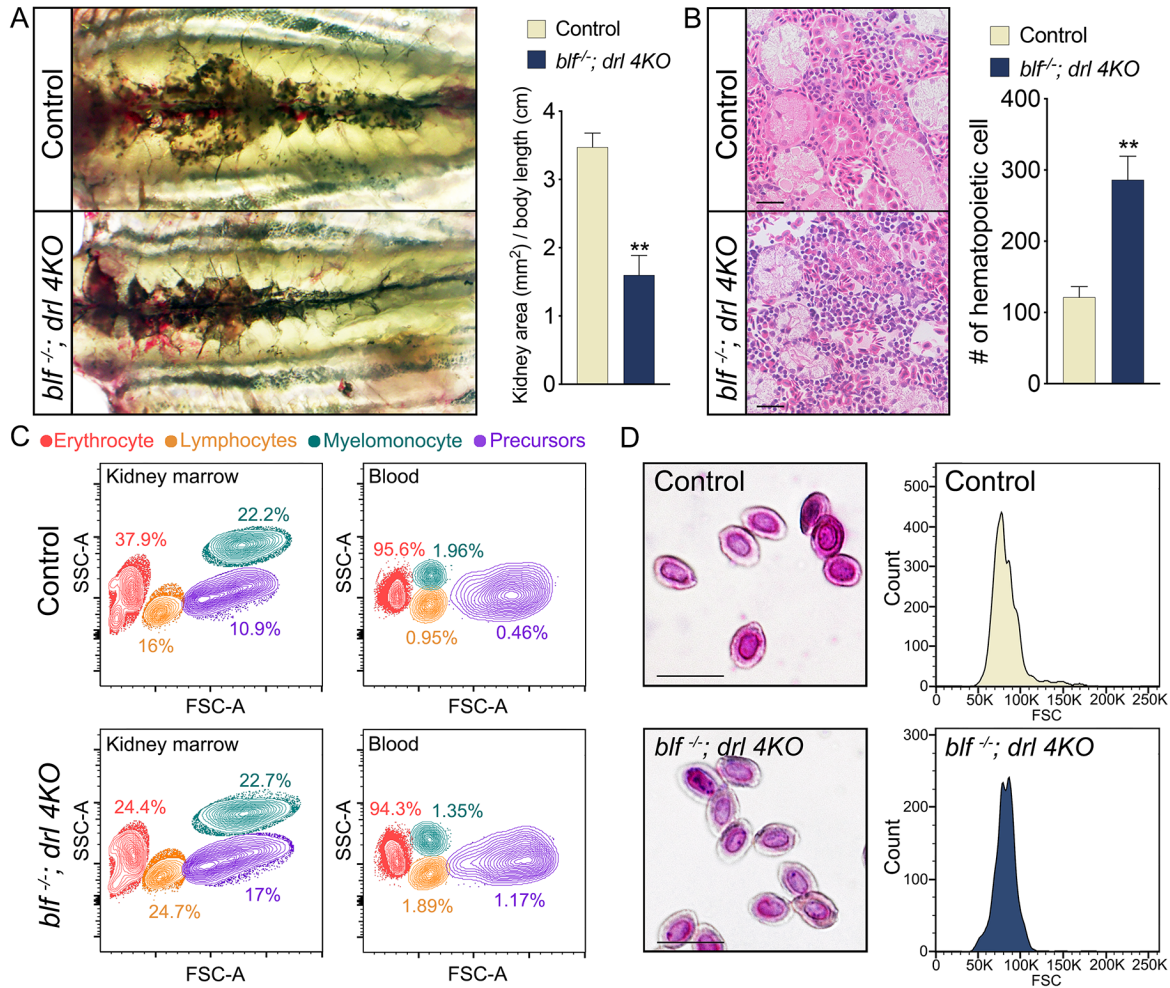


Fig. S3. Microscopic observation and hematological analysis of adult *blf*^{-/-}; *drl* 4KO fish. **(A)** Left panels, brightfield images of adult zebrafish kidney. The retroperitoneal hematopoietic kidney tissue appears as a dark flattened structure. Kidney size were measured and are reported relative to body length. **(B)** Photomicrographs of hematoxylin and eosin stained sections of head kidneys. Hematopoietic cells could be found between the renal tubules. Scale bar: 20 μ m. Number of hematopoietic cells was counted on a 150 μ m x150 μ m field. **(C)** Representative flow cytometry plots from single cell suspensions from the dissected kidney and peripheral blood. Forward scatter (FSC) and side scatter (SSC) are proportional to cell size and cellular granularity, respectively. Four major populations were delineated: erythroid (red), lymphoid/erythroblast (brown), myeloid (green), and the immature precursor cells (purple). **(D)** Left panels, Wright-Giemsa staining of peripheral blood cells from adult zebrafish. Red blood cells are

terminally differentiated with elliptical morphology and condensed nuclei. Scale bar: 10 μm . Right panels, mean cell volume of red blood cells of adult control and *b1f*^{-/-}; *drl* 4KO fish, cells from 2 genotypes have a similarly distributed volume. A, B, C and D at least 6 fish from each genotype were examined and representative results are shown. A and B, data are mean \pm SEM, **P<0.01.

Supplemental Figure 4

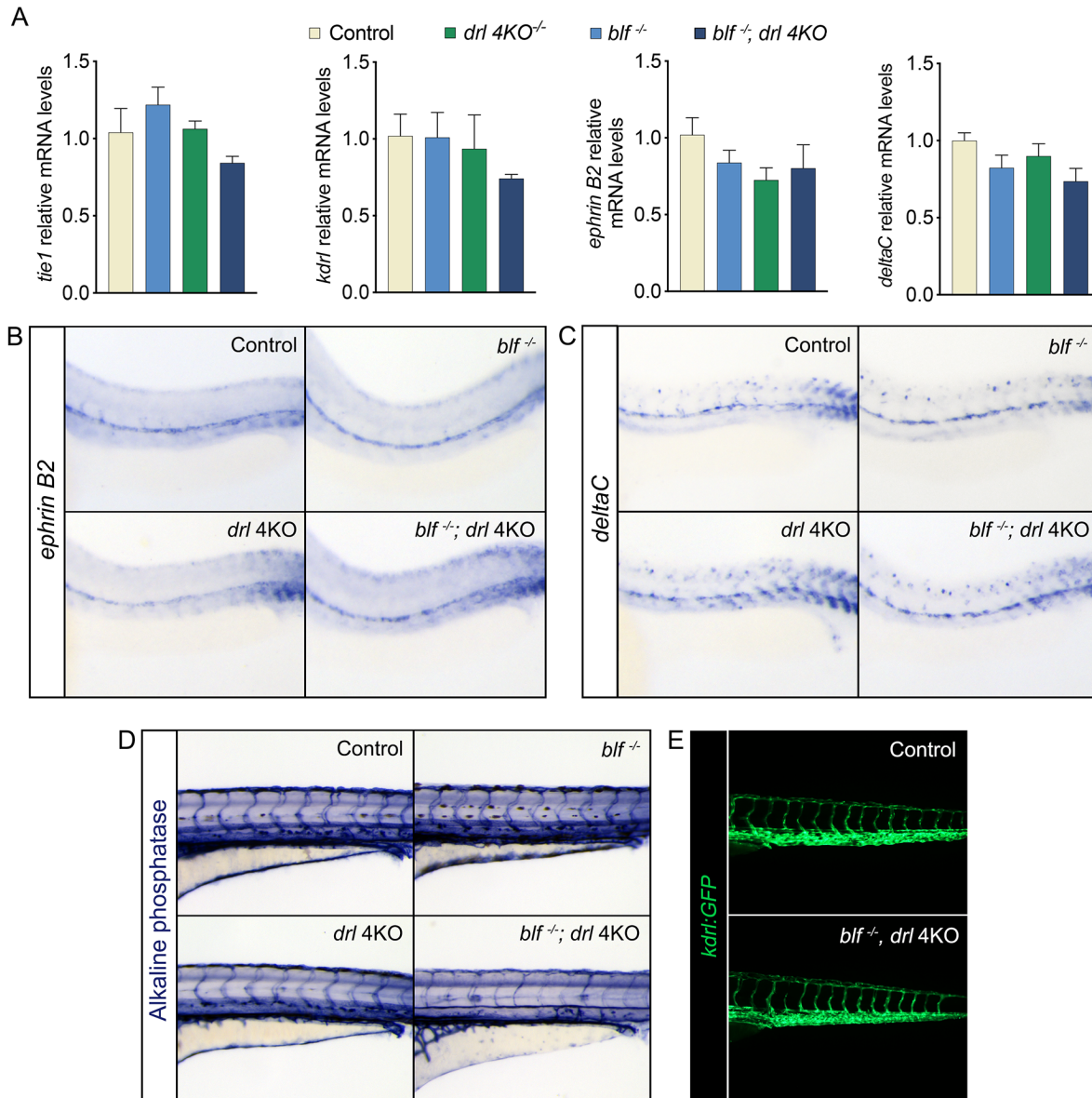


Fig. S4. *Blf* and *drl* cluster genes are dispensable for vasculature development. **(A)** QPCR results for the expression of *tie1*, *kdrl*, *ephrin B2* and *deltaC*. *Tie1* and *kdrl* are examined at 8 somite stage, *ephrin B2* and *deltaC* are examined at 24 hpf. Data are mean \pm SEM of at least three replicates. **(B)** RNA *in situ* hybridization results for the expression of *ephrin B2* and *deltaC* in 24 hpf embryos. Lateral view with head to left. For *ephrin B2* WISH, n=38, 31, 39 and 33 for each genotype. For *deltaC* WISH, n=32, 37, 39 and 35 for each genotype. **(D)** Alkaline phosphatase

staining reveals the structure of intersegmental vessels at 72 hpf, n=32, 29, 28 and 30 for each genotype. (E) Fluorescence micrographs of wild type and *b1f*^{-/-}; *drl* 4KO embryos in Tg(*kdr1:eGFP*) transgenic background 72 hpf. In comparison with wild type embryos, *b1f*^{-/-}; *drl* 4KO embryo display similar patterns of intersegmental vessel and caudal vein. D and E, at least 8 embryos from each genotype were examined and representative results are shown.

Supplemental Figure 5

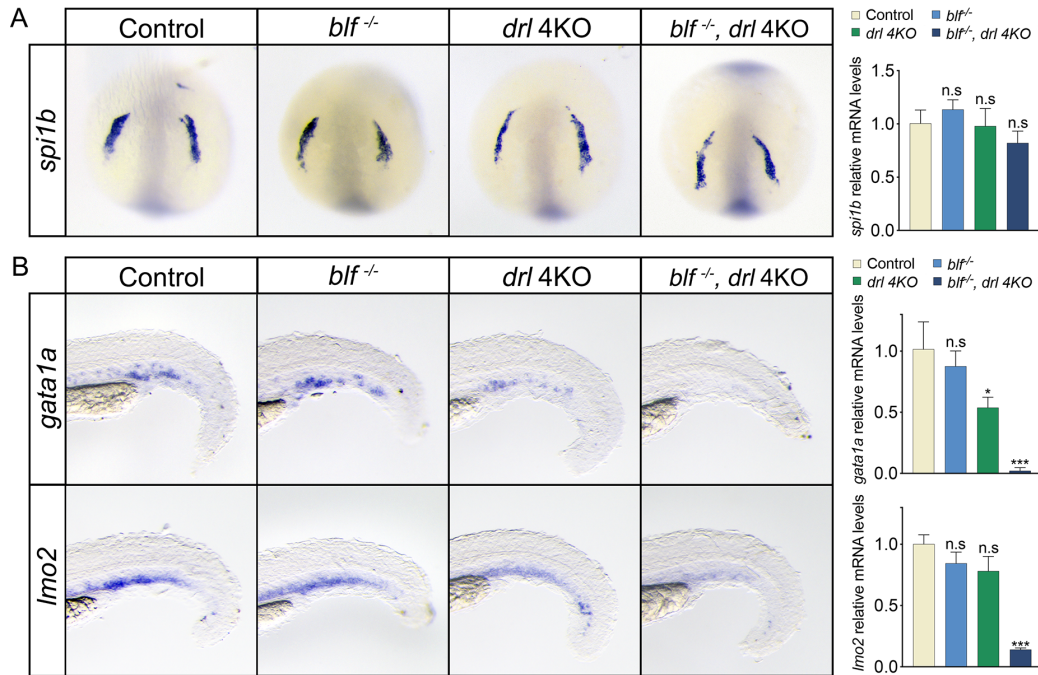


Fig. S5. The effect of loss of *blf* and *drl* cluster genes on primitive myelopoiesis and the formation of erythromyeloid progenitors. **(A)** RNA in situ hybridization and qPCR results for expression of *spi1b* in 8 somite embryos, n=26, 33, 31 and 40 for each genotype. Data are mean \pm SEM of at least three replicates. n.s., not significant. **(B)** RNA in situ hybridization and qPCR results for expression of *gata1a* (n=39, 35, 31 and 27) and *lmo2* (n=34, 30, 26 and 32) in 30 hpf embryos. Data are mean \pm SEM of at least three replicates. n.s., not significant, ***P<0.001.

Supplemental Figure 6

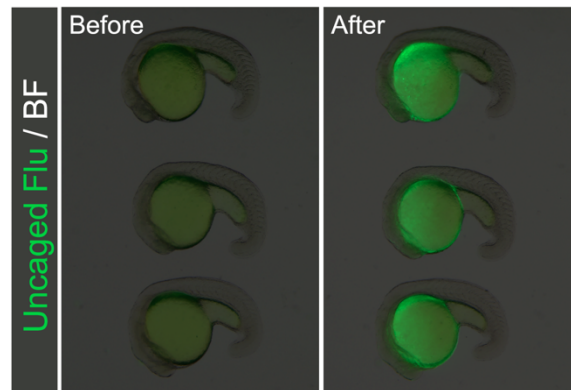


Fig. S6. *In vivo* rostral myeloid progenitors labeling with a photoactivatable cell tracer. At 20 hpf, after injection of caged fluorescein in the embryo at the 1-cell stage, the fluorescein in anterior part of embryo was uncaged with a pulsed ultraviolet [365 nm] laser beam.

Supplemental Figure 7

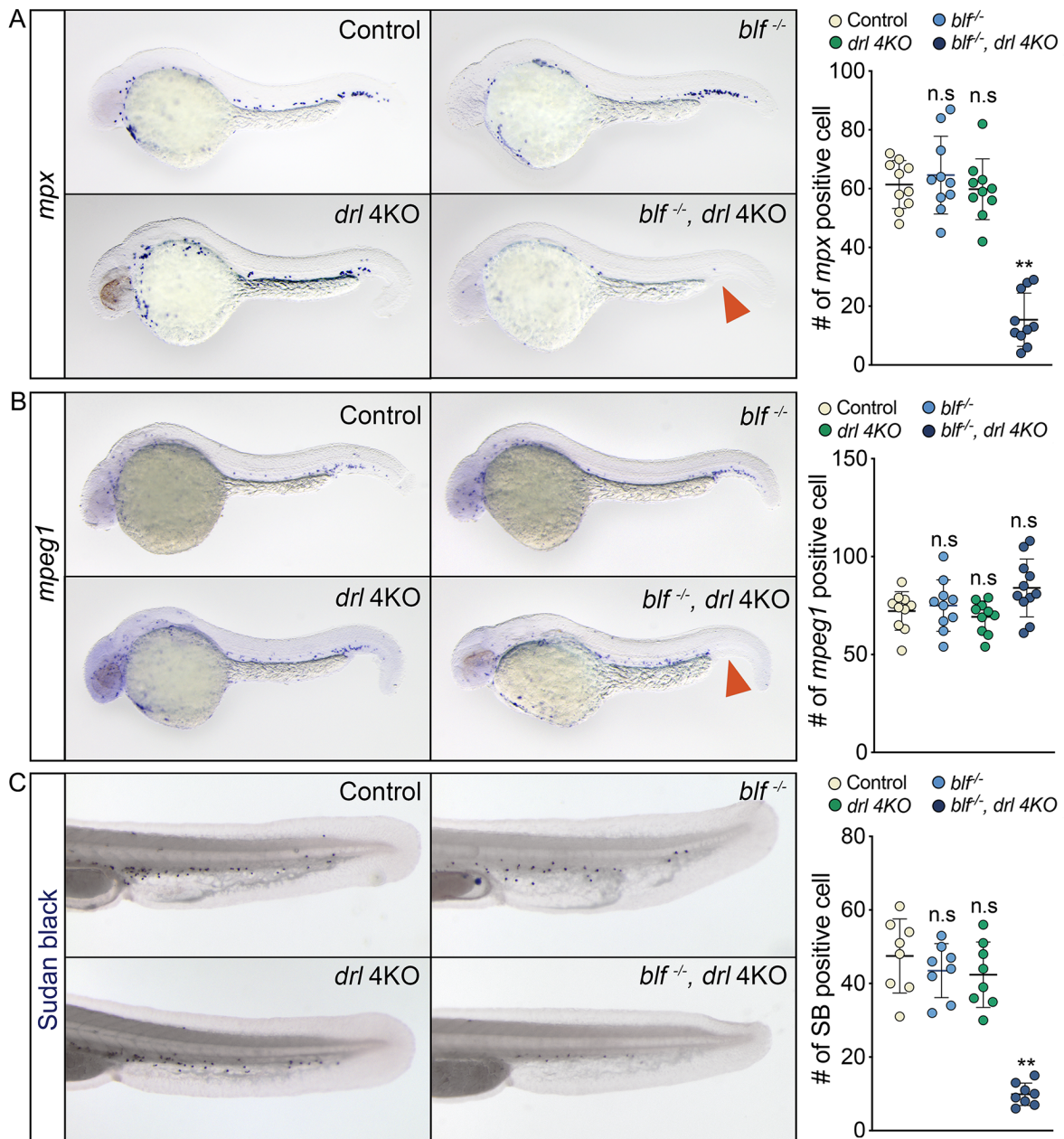


Fig. S7. The effect of loss of *blf* and *drl* cluster genes on intermediate myelopoiesis. **(A)** Left panels, RNA *in situ* hybridization results for expression of *mpx* in 36 hpf embryos. Right panel, scatter plot showing the mean number of *mpx*+ cells. **(B)** Left panels, RNA *in situ* hybridization results for expression of *mpeg1* in 36 hpf hpf embryos. Right panel, scatter plot showing the mean number of *mpeg1*+ cells. Red arrowheads in A and C indicates the lack of *in situ* hybridization

signal in posterior blood island (PBI). **(C)** Left panel, Sudan Black B (SB) staining of neutrophils in the CHT region in embryos at 36 hpf. Right panel, scatter plot showing the mean number of SB+ neutrophils. A, B and C, data are mean \pm SEM, n.s, not significant, **P<0.01, ***P<0.001.

Supplemental Figure 8

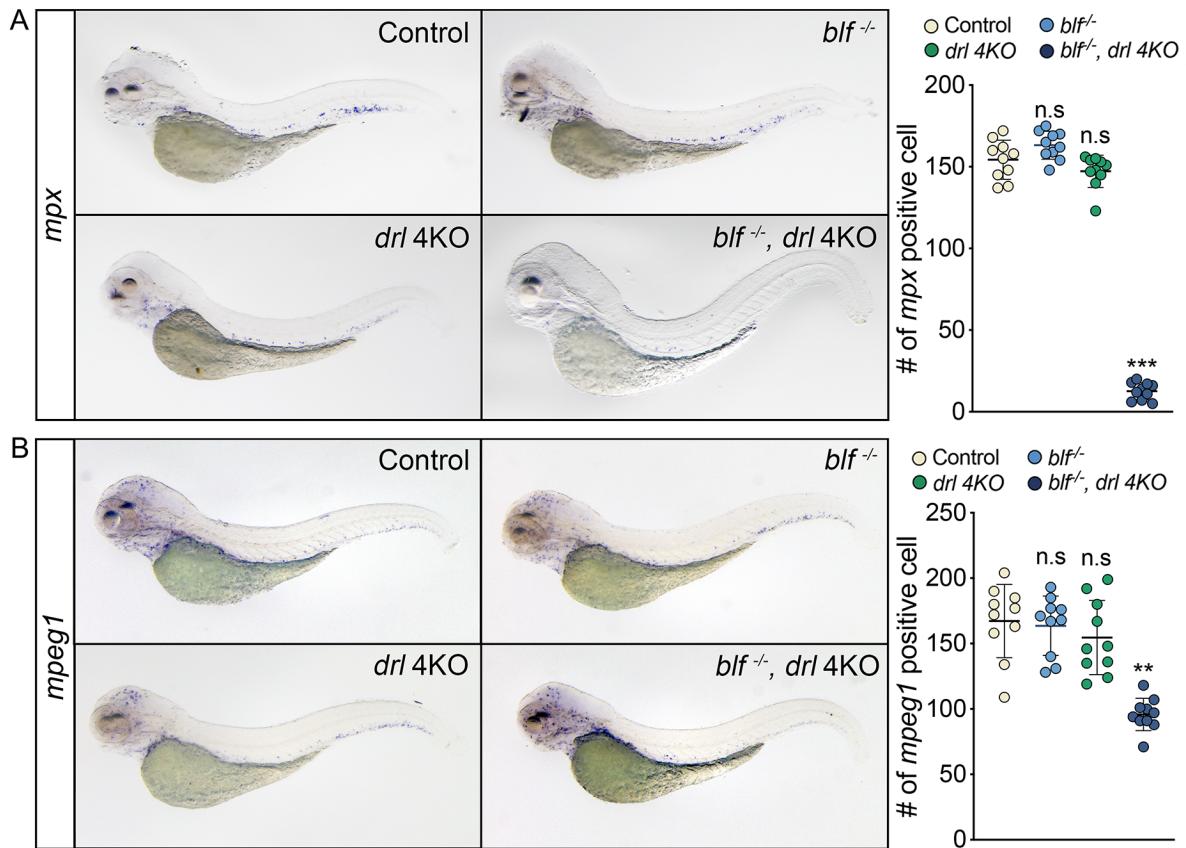


Fig. S8. The effect of loss of *blf* and *drl* cluster genes on definitive myelopoiesis. **(A)** Left panels, RNA *in situ* hybridization results for expression of *mpx* in 96 hpf embryos. Right panel, scatter plot showing the mean number of *mpx*⁺ cells. **(B)** Left panels, RNA *in situ* hybridization results for expression of *mpeg1* in 96 hpf embryos. Right panel, scatter plot showing the mean number of *mpeg1*⁺ cells. A and B, data are mean \pm SEM. n.s, not significant. **P<0.001, ***P<0.0001.

Supplemental Figure 9

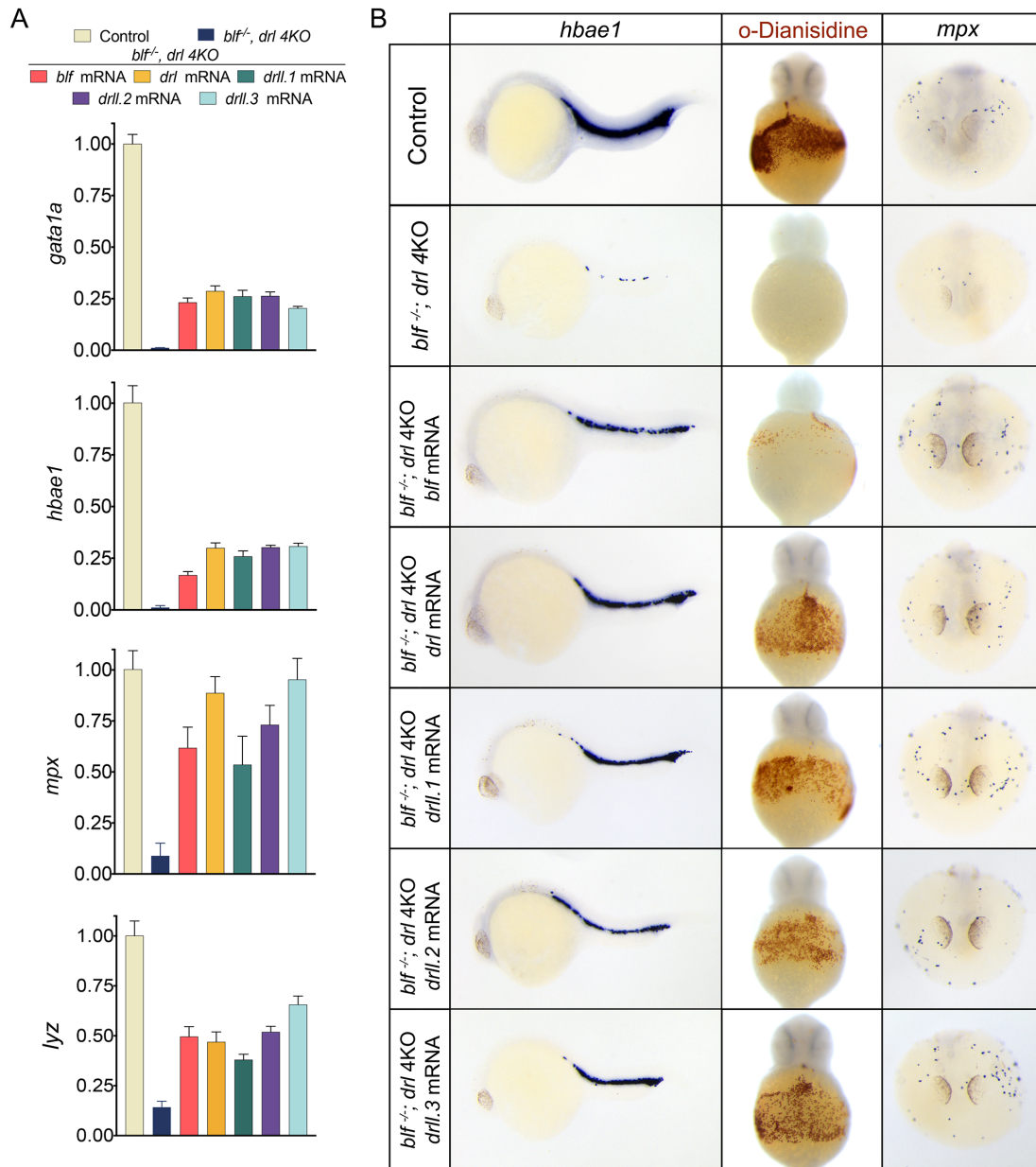


Fig. S9. *Bif* and *drl* cluster genes redundantly regulate zebrafish haematopoiesis. **(A)** QPCR results for expression of marker genes at 23 hpf in $bif^{-/-}; drl\ 4KO$ embryos after mRNA injection. Data are mean \pm SEM of at least three replicates. **(B)** Left panel, expression of *hbae1* in $bif^{-/-}; drl\ 4KO$ embryos at 24 hpf embryos after mRNA injection, n=27, 39, 39, 36, 40, 30 or 38 for each experimental group. Lateral view with head to left. Middle panel, whole-mount O-dianisidine staining of 36 hpf embryos, ventral views, n=30, 37, 38, 31, 37, 31 or 37 for each experimental

group. Right panel, RNA *in situ* hybridization results for expression of *mpx* in primitive neutrophils in 24 hpf embryos, frontal view, n=39, 32, 33, 33, 33, 39 or 33 for each experimental group.

Supplemental Figure 10

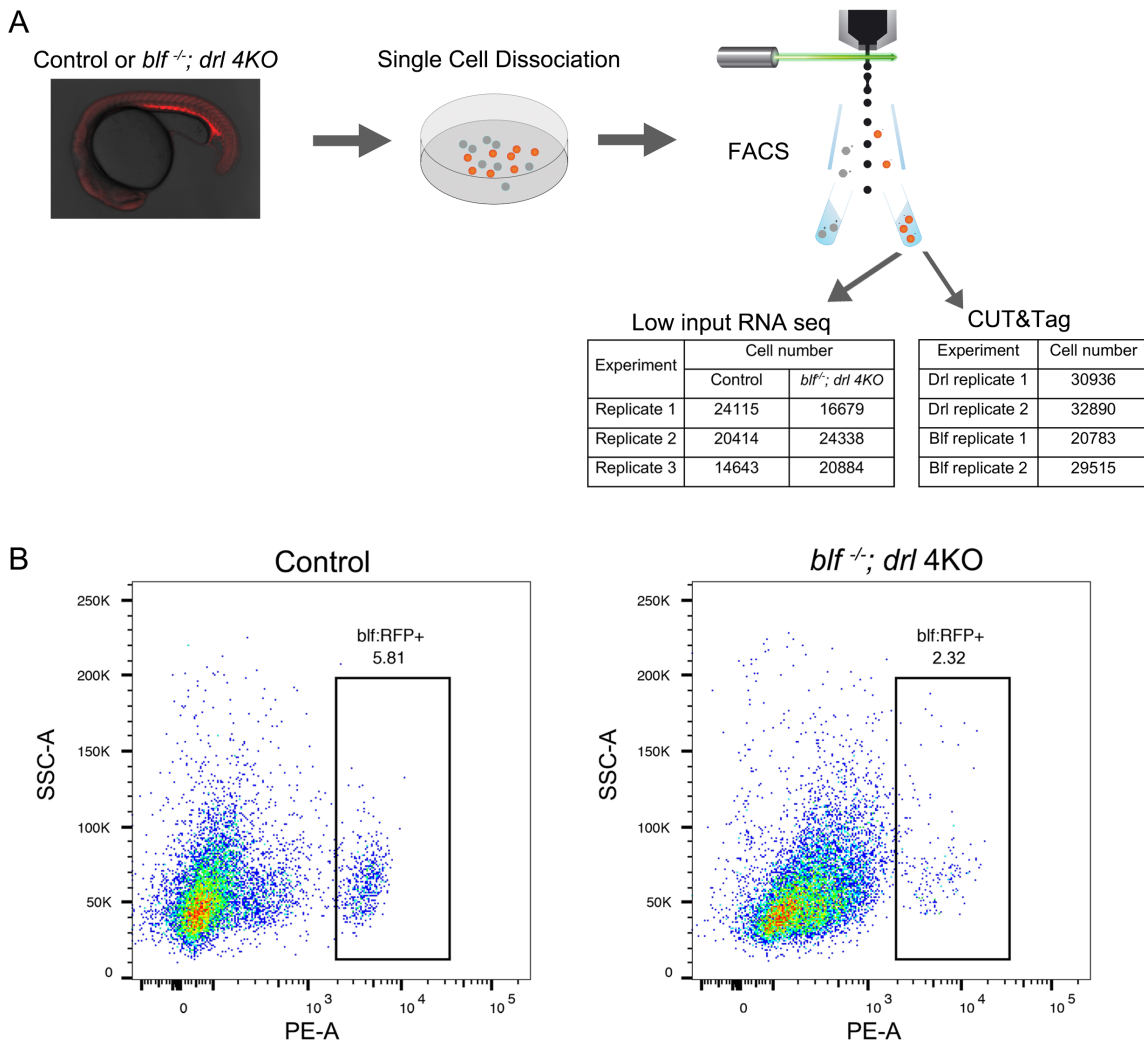


Fig. S10. Isolation and profiling of hematopoietic progenitors from control and *blf*^{-/-}; *drl* 4KO embryos. **(A)** Schematic of cell preparation. At 20 hpf, the whole embryo was dissociated into single cells, then RFP+ hematopoietic progenitors were isolated by FACS for downstream low input RNA sequencing or CUT&Tag sequencing. **(B)** Representative FACS plots of single cells with RFP fluorescence on the x-axis and side scatter area on the y-axis. RFP+ population (5.81% in control sample and 2.32% in *blf*^{-/-}; *drl* 4KO sample) displayed strong separation from the RFP- population.

Supplemental Figure 11

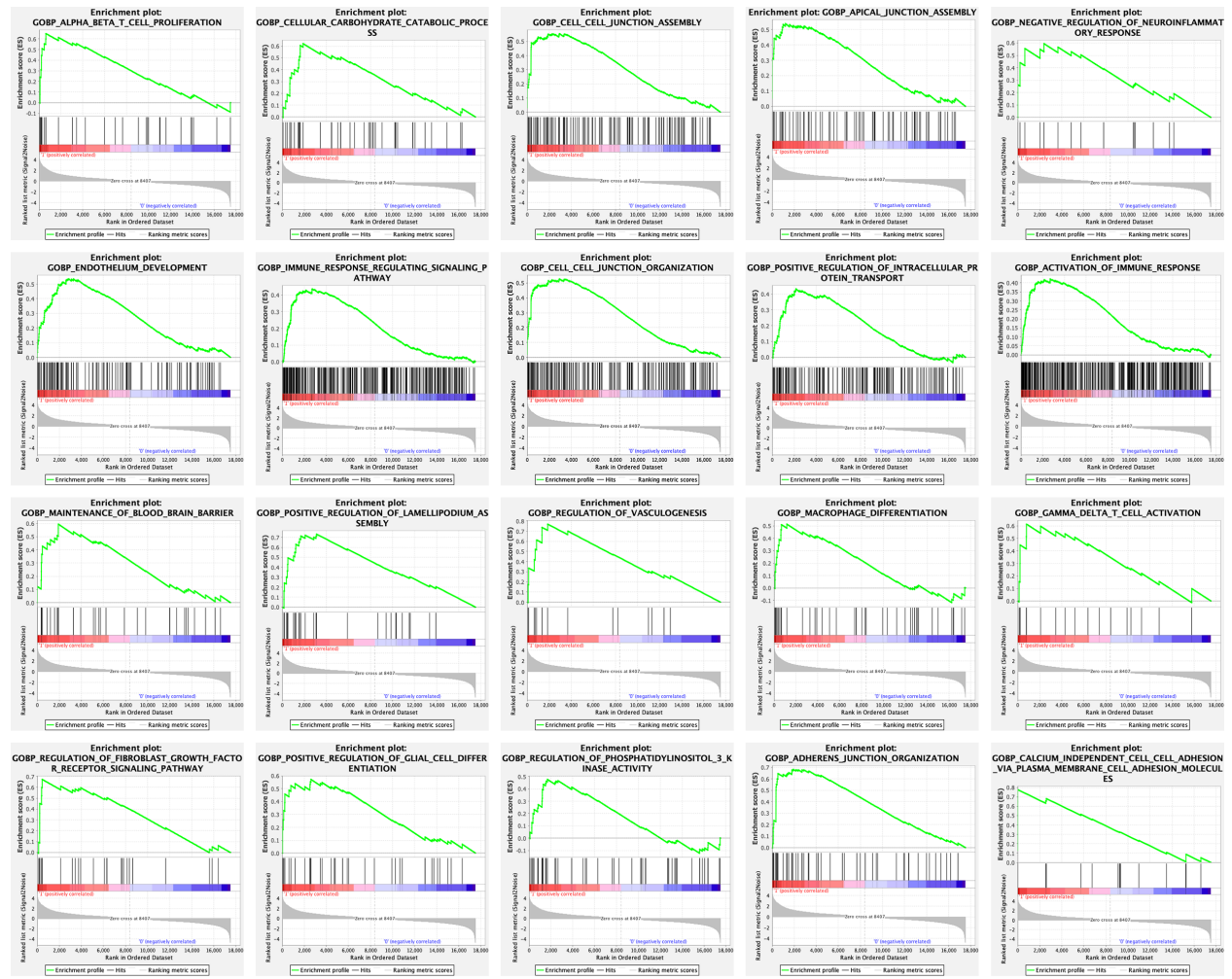


Fig. S11. GSEA analysis of the transcriptome dataset from control and *btf^{-/-}; dri 4KO* samples. Gene sets were ranked based on normalized enrichment score (NES) and top 20 sets were displayed.

Supplemental Figure 12

Transcription factor	Motif	p-value	% of targets	% of background
ZKSCAN1		1e-27	4.66%	1.40%
Gata3		1e-20	7.23%	1.78%
Stat3		1e-11	13.29%	4.91%
CEBP		1e-10	14.65%	11.65%
Gata1		1e-9	8.82%	2.90%
Klf1		1e-9	5.10%	3.38%
ZBTB33		1e-9	25.60%	9.59%
Nrf1		1e-9	11.16%	3.47%
Fosl2		1e-8	13.29%	5.38%
Klf4		1e-8	16.31%	4.11%

Fig. S12. Enriched sequence motifs identified by HOMER known motif analysis at Blf and Drl co-occupancy sites. The top 10 motifs are shown.

Supplemental Figure 13

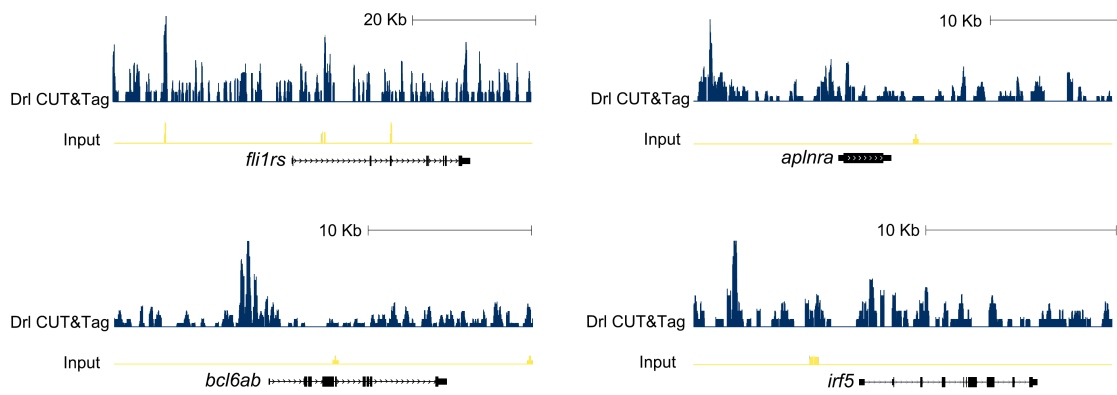


Fig. S13. Genome browser views of Drl binding profiles associated with *fli1rs*, *aplnra*, *bcl6ab* and *irf5*.

Supplemental Figure 14

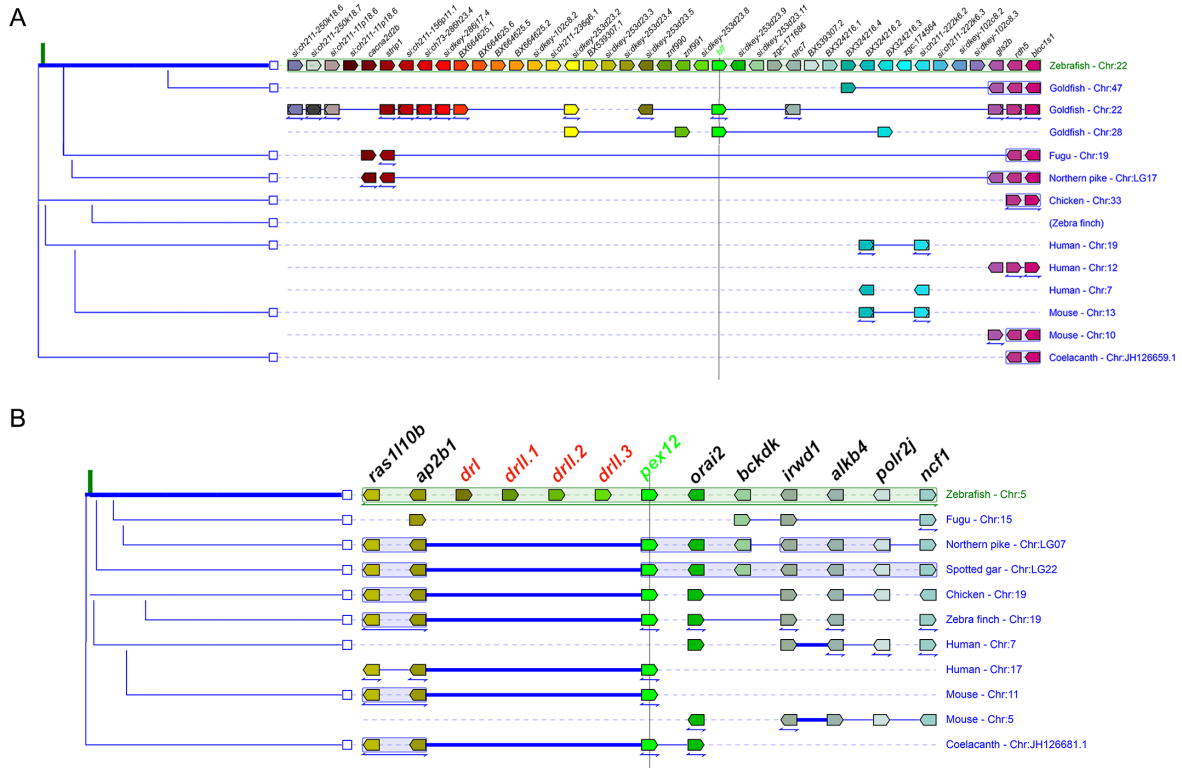


Fig. S14. Cross-species synteny analysis of *blf* and *drl* cluster. **A** and **B**, synteny diagram of the *blf* and *drl* cluster in zebrafish compare to other vertebrate animals.

Supplemental Figure 15

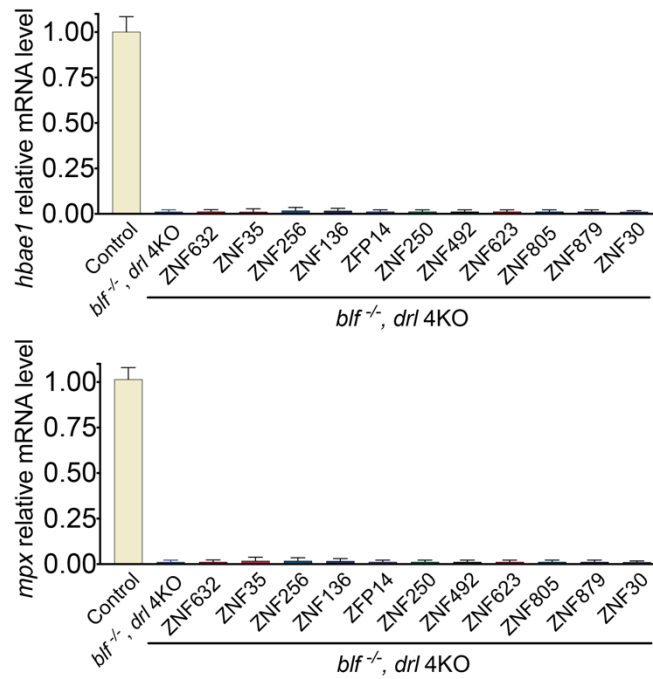


Fig. S15. Screening the mammalian functional ortholog of zebrafish *blf* and *drl* cluster genes. QPCR results for expression of erythroid mark genes *hbae1* and neutrophil marker gene *mpx* in *blf*^{-/-}; *drl* 4KO embryos after mRNA injection. Data are mean \pm SEM of at least three replicates.

Supplemental Figure 16

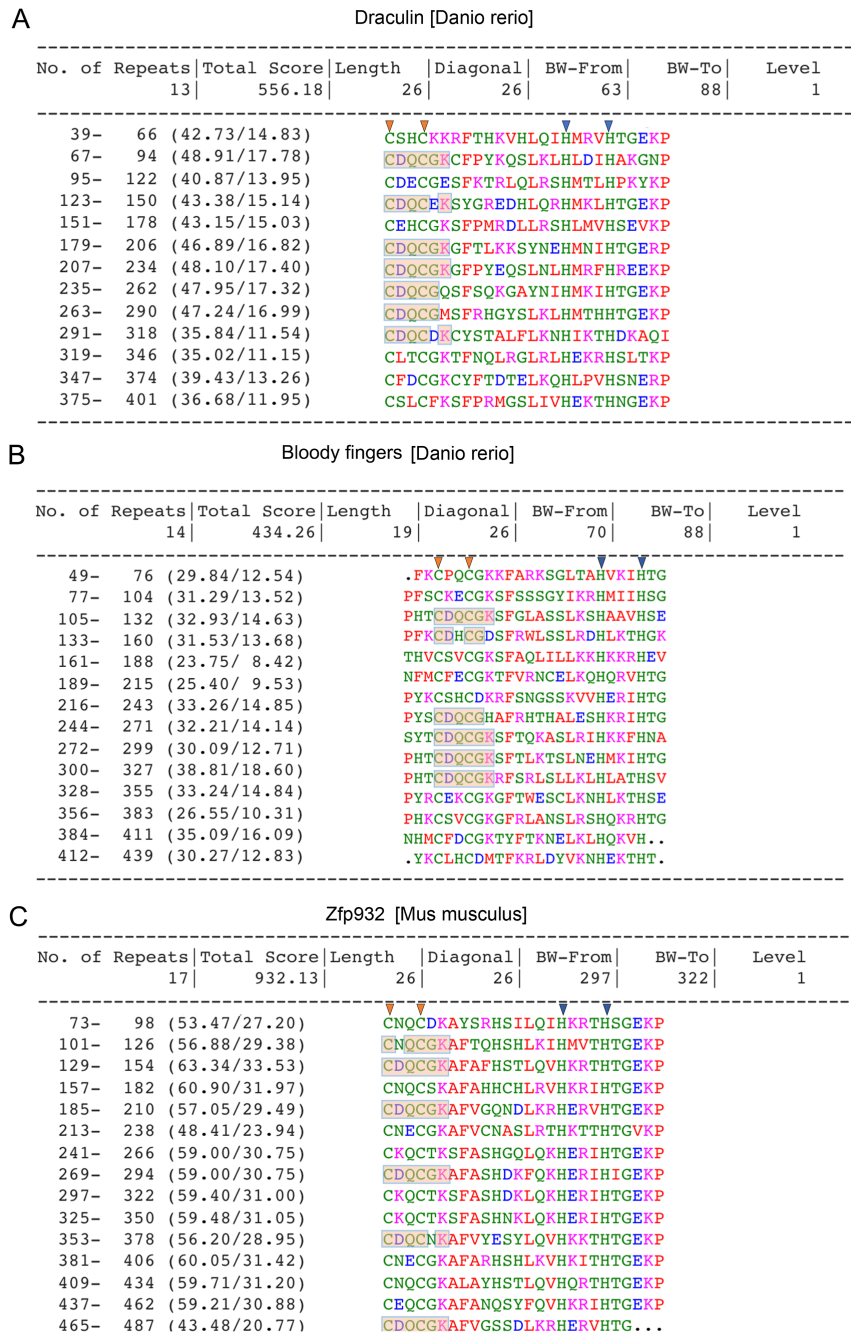


Fig. S16. Repeated sequence motifs of Drl, Blf and Zfp932 identified by RADAR. BW, best window. Orange and blue arrowheads indicate the cysteine and histidine residues on C2H2 Zinc finger.

Table S1. Differential expression genes between *blf*^{-/-},drl 4KO and control cells.

[Click here to download Table S1](#)

Table S2. List of Drl and Blf binding regions in blf:RFP+ cells.

[Click here to download Table S2](#)

Table S3. List of direct downstream genes of Drl.

[Click here to download Table S3](#)

Table S4. Mammalian ortholog candidates of zebrafish *bif* and *drl* cluster genes

Name	NCBI Ref. Seq	E-value	Secondary Structure Scores	Aligned cols	Target Length
ZNF266	NP_006622.2	1.70E-49	36.6	398	549
ZNF101	NP_001287878.1	1.00E-48	35.4	316	316
ZNF632	XP_047297102.1	1.80E-49	34.8	409	543
ZNF226	NP_001027545.1	1.00E-48	34.8	408	803
ZFP932	NP_663538.2	1.60E-49	34.6	411	526
ZNF35	NP_003411.3	1.00E-48	34.4	406	527
ZNF256	NP_001362332.1	2.10E-49	34.2	396	474
ZNF136	NP_001334943.1	4.50E-49	34.2	369	508
ZFP2	NP_085116.2	3.40E-49	34.1	410	461
ZFP14	NP_001284548.1	5.40E-49	34.1	394	534
ZNF184	NP_001305820.1	5.70E-49	34.1	409	751
ZNF180	NP_001265438.2	1.00E-48	34	409	665
ZFP345	NP_001030072.2	1.30E-49	33.9	398	561
ZFP950	NP_001296145.1	8.20E-49	33.8	408	609
ZFP184	NP_898835.1	1.30E-49	33.3	406	737
ZNF345	NP_001229401.1	3.00E-49	33	403	488
ZNF595	NP_872330.1	7.60E-49	32.5	391	648
ZNF250	NP_001103159.1	6.10E-49	31.2	394	555
ZNF492	NP_065906.1	9.90E-49	29.9	401	531
ZNF623	NP_001075949.1	5.40E-49	29.4	405	496
ZNF805	NP_001138550.1	6.10E-49	29	411	494
ZNF879	NP_001129588.1	1.30E-49	28.6	392	563
ZNF30	NP_001307595.1	1.30E-49	28.4	395	519
ZNF429	NP_001333842.1	1.00E-48	26.7	395	642

Candidates were ranked according to secondary structure scores . Aligned Cols', lengths of the aligned region. Target Length, lengths of the candidate protein.

Table S5. Primers for quantitative real-time RT-PCR analysis.

[Click here to download Table S5](#)